Remote Sens. **2013**, *5*, 5725-5756; doi:10.3390/rs5115725

OPEN ACCESS

Remote Sensing

ISSN 2072-4292

www.mdpi.com/journal/remotesensing

Article

Polarimetric Parameters for Growing Stock Volume Estimation Using ALOS PALSAR L-Band Data over Siberian Forests

Tanvir Ahmed Chowdhury *, Christian Thiel, Christiane Schmullius and Martyna Stelmaszczuk-Górska

Department of Earth Observation, Friedrich-Schiller-University Jena, Loebdergraben 32, D-07743 Jena, Germany; E-Mails: christian.thiel@uni-jena.de (C.T.); c.schmullius@uni-jena.de (C.S.); m.stelmas@uni-jena.de (M.S.-G.)

***** Author to whom correspondence should be addressed; E-Mail: tanvir-ahmed.chowdhury@uni-jena.de; Tel.: +49-364-1948-978; Fax: +49-364-1948-882.

Received: 10 September 2013; in revised form: 19 October 2013 / Accepted: 24 October 2013 / Published: 4 November 2013

Abstract: In order to assess the potentiality of ALOS L-band fully polarimetric radar data for forestry applications, we investigated a four-component decomposition method to characterize the polarization response of Siberian forest. The decomposition powers of surface scattering, double-bounce and volume scattering, derived with and without rotation of coherency matrix, were compared with Growing Stock Volume (GSV). To compensate for topographic effects an adaptive rotation of the coherency matrix was accomplished. After the rotation, the correlation between GSV and double-bounce increased significantly. Volume scattering remained same and the surface scattering power decreased slightly. The volume scattering power and double-bounce power increased as the GSV increased, whereas the surface scattering power decreased. In sparse forest, at unfrozen conditions the surface scattering was higher than volume scattering, while volume scattering was dominant in dense forest. The scenario was different at frozen conditions for dense forest where the surface scattering was higher than volume scattering. Moreover, a slight impact of tree species on polarimetric decomposition powers has been observed. Larch was differed from aspen, birch and pine by +2 dB surface scattering power and also by −1.5 dB and −1.2 dB volume scattering power and double-bounce scattering power respectively at unfrozen conditions.

Keywords: four-component decomposition power; growing stock volume; tree species; weather conditions; Siberia; L-band

1. Introduction

Siberian forests, which contain roughly half of the world's Growing Stock Volume (GSV) of coniferous species [1], and play an important role as a carbon sink [2], suffer from several types of disturbances. Much of this damage is caused by immense wood trade, illegal logging, and also rigorous damages due to fires, insects and air particulate pollution. The GSV is defined as the stem volume of all living trees including bark but excluding branches and stamps in a stand. The trees must be greater than 6 cm at breast height (1.3 m) to be included in growing stock.

The forest degradation or deforestation has an impact on climate change. Therefore, it is necessary to monitor Siberian forests on a large-scale, frequently, and accurately. The traditional ground survey is useful for the local investigations but taking into account the vastness and remoteness of Siberian forests and also not sufficient infrastructure, forest inventories are not carried out frequently enough to provide the information about the ecosystem. Moreover, ground-based surveys are too expensive and time consuming. Possible solution to overcome this problem is to use remote sensing, in particular space-borne remote sensing techniques. In Siberia, the optical remote sensing data are affected by frequent cloud cover, fog, mist, or darkness over the long periods of the year. Microwave remote sensing technique of lower frequency radar sensor, which is not sensitive to cloud cover and solar radiation, provides efficient means to accomplish this task, especially by combining polarimetric techniques. Moreover, SAR can provide a global view of the whole Siberian forests area with high temporal resolution. Due to their sensitivity to the geometric properties of the targets, radar data proved to have a strong potential for forest biomass assessment. Lower frequencies (L-band and P-band) are more preferable than higher frequencies (X-band and C-band) as saturation emerges at higher biomass levels [3–5], *i.e.*, after a specific biomass level the further increase of biomass causes no further increase of the radar backscattering intensity. Additionally, radar backscattering at high frequencies is dominated by the scattering process in the crown layer of small branches, needles, twigs, and therefore, it does not penetrate and scatter significantly from the stem, while backscatter at lower frequencies is dominated by the scattering process from the trunks and large branches in which almost 70% of the total living biomass of forest is accumulated [6].

1.1. Polarimetric SAR in Forestry Applications

Radar polarimetry is the science of acquiring, processing and analyzing the polarization state of an electromagnetic field [7]. Radar polarimetry deals with the full vector nature of polarized electromagnetic waves. When the wave passes through a medium strikes an object, it is reflected; then, characteristic information about its geometrical structure such as reflectivity, shape and orientation and its geophysical properties can be obtained. PolSAR data expresses the changes of polarization states of received microwave by the structures and dielectric constant of the objects. A fully polarimetric dataset comprises both, co- and cross-polarization defined in an orthogonal polarization basis. This most of all

cases, the antenna transmits and receives horizontally and vertically polarized signals. Therefore, a single set of PolSAR image consists of four complex images of different polarization combinations, *i.e*., HH- (transmits and receives horizontally polarized signals), HV- (transmits horizontally polarized signals, receives vertically polarized signals), VH-, and VV-polarization images. Superior objective of polarimetric data exploration is the analysis of backscattering mechanisms of scattering objects and thus to gain insight into their physical characteristics and can be used to distinguish the scattering objects. Basic data examination techniques analyze polarimetric coherence or polarimetric phase difference. Both parameters allow first implications on the scattering processes [8] and have been successfully implemented to improve forest biomass estimation [3].

Apart from the polarimetric phase difference and polarimetric coherence, a number of decomposition approaches have been designed [9–12]. The single components of the backscattering signal can be assigned to specific scattering processes such as surface scattering, volume scattering and double-bounce. So far, the effort has been focused on land cover classification [12–16] and the delineation of physical land surface parameters such as soil moisture and surface roughness [17–22].

McNeil *et al.* [23] and Garestier *et al.* [24] considered Cloude-Pottier decomposition [10] parameters for the estimation of forest stand age and tree height. The authors found correlation between decomposition parameters and forest stand age as well as tree height. Baker *et al.* [25] and Watanabe *et al.* [26] investigated the scattering mechanism in temperate and boreal forests. The authors were able to separate the forest response into fractional contributions from the three broad classes of scattering mechanisms double-bounce, surface and volume scattering and found the dominance of surface scattering and volume scattering in sparse forest and dense forest respectively. Goncalves *et al.* [27] and Kobayashi *et al.* [28] applied Freeman-Durden decomposition [12] and Yamaguchi decomposition method [29] respectively in tropical forest. Goncalves *et al*. [27] observed the strong correlation between GSV and surface scattering (r = 0.49), double-bounce (r = 0.63) and volume scattering (r = 0.61). Kobayashi *et al*. [28] also found that all of the decomposition powers have more significant correlations with the forest parameters when divided by the total power ($r \approx -0.768$ for surface scattering, $r \approx 0.558$ for double-bounce scattering and $r \approx 0.709$ for volume scattering) rather than when using the decomposition powers themselves ($r \approx -0.722$ for surface scattering, $r \approx -0.028$ for double-bounce scattering and $r \approx 0.513$ for volume scattering).

1.2. Motivation and Scope

Although above mentioned studies have reported results showing a strong potential of polarimetric decomposition parameters for retrieving forest biophysical parameters, the analyses were based on a limited set of images and were focused on limited number of test areas. The effect of environmental conditions on polarimetric decomposition parameters was not assessed. Furthermore, the studies could not confirm the findings for large areas. Furthermore, only intensively managed and homogenous forest stands have investigated. Some studies have shown the potential of tree species discrimination based on polarimetric data [26,30]. Watanabe *et al*. [26] applied Freeman-Durden decomposition model to the L-band polarimetric SAR data in Tomakomai national forest, Japan where the main tree species are fir, larch, spruce and some percentage of broadleaf species are also available. The authors investigated that larch has higher contribution of surface scattering and lower contribution of

double-bounce and volume scattering. Ranson *et al*. [30] discovered C-, L-, P-band AIRSAR data better enabled for discriminating deciduous forest whereas SIR-C/X data produced better classification results for conifer forest stands. However, the impact of tree species on decomposition powers has not yet been fully examined in these studies.

The aim of this study is to gain knowledge in terms of polarimetric properties in Siberian forests and to investigate the potential of ALOS PALSAR L-band polarimetric decomposition powers, in particular double-bounce, surface, and volume scattering for the estimation of GSV. In addition, the sensitivity for different weather conditions will be addressed. A further objective is the examination of different tree species on decomposition powers. The study is focused on GSV, as it is the key parameter in Russian forest inventories for planning forest enterprise operations. Moreover, in the context of Global Climate Change, forest biomass is the one of the most desired forest parameters. Forest inventories delivered by foresters usually include GSV. Therefore, the knowledge about GSV allows the estimation of above ground biomass through forest type and forest age specific conversion factors [31]. The test areas are chosen for a number of reasons: availability of SAR imagery, forest inventory, and meteorological data. The vastness of these forest areas represents the full diversity of the land cover. The forested areas have been considered in previous investigations for the retrieval of forest biophysical parameters using SAR remote sensing techniques [6,32–37]. During the past 15 years, much effort has been made in regard to the forestry applications using PolInSAR (Polarimetric Interferometry SAR) techniques [38–41]. However, in this study we solely concentrate on the polarimetric information. Rationale is the absence of an adequate global PolInSAR dataset (L- or P-band, single pass), while polarimetric ALOS PALSAR data exist for a high percentage of the globe.

This paper is structured as follows: after the description of the test areas, satellite data and data processing we present the analysis of the behavior of the polarimetric decomposition powers as a function of GSV, weather conditions, and different tree species in Siberian forests. The important part of this investigation is to determine the existence of correlation between the polarimetric decomposition powers and GSV and to examine the seasonal variability. Subsequently, we present an approach for estimating the GSV based on polarimetric decomposition powers.

1.3. Theoretical Background

The backscatter properties of the target can be completely described by a scattering matrix [*S*]. The [*S*] matrix is only able to characterize the polarimetric behavior of point scatterers. But for remote sensing applications the scatterers are affected by spatial and time variations and can only be characterized with the presence of speckle noise. A resolution cell in a SAR image is coarser than the wavelength of the radar and the cell is composed of many distributed deterministic scatterers. Each of the scatterers is represented by an individual Sinclair matrix $[S]_i$. Therefore, the matrix [*S*] is formed by the coherent addition of the individual $[S]_i$ matrices for all the distributed scatterers within each resolution cell. To reduce the speckle effect second order polarimetric representation such as covariance matrix or coherency matrix is introduced.

1.3.1. Covariance and Coherency Matrix

The covariance matrix [*C*] is formed by the outer product $\langle \overrightarrow{\boldsymbol{k_L}}.\overrightarrow{\boldsymbol{k_L}}^{+} \rangle$ of the lexicographic scattering vector $\langle \overrightarrow{\boldsymbol{k_L}} \rangle$ with its conjugate transpose vector $\langle \overrightarrow{\boldsymbol{k_L}}^{+} \rangle$.

$$[C] = \langle \overrightarrow{k_L}.\overrightarrow{k_L}^{+} \rangle = \begin{bmatrix} \langle |S_{HH}|^2 \rangle & \sqrt{2}\langle S_{HH}S_{HV}^{*} \rangle & \langle S_{HH}S_{VV}^{*} \rangle \\ \sqrt{2}\langle S_{HV}S_{HH}^{*} \rangle & \langle |S_{HV}|^2 \rangle & \sqrt{2}\langle S_{HV}S_{VV}^{*} \rangle \\ \langle S_{VV}S_{HHVV}^{*} \rangle & \sqrt{2}\langle S_{VV}S_{HV}^{*} \rangle & \langle |S_{VV}|^2 \rangle \end{bmatrix} \quad (1)$$

where $\langle ... \rangle$ represents ensemble averaging assuming that the spatial scattering medium to be averaged is homogenous. The diagonal elements correspond to the backscattered intensities. The off diagonal elements represent the complex covariance of the respective polarization configurations. Similarly, the coherency matrix [*T*] is defined by the other product $\langle \overrightarrow{k_P}.\overrightarrow{k_P}^{+} \rangle$ of the Pauli scattering vector:

$$[T] = \langle \overrightarrow{k_P}.\overrightarrow{k_P}^{+} \rangle \begin{bmatrix} \langle |S_{HH} + S_{VV}|^2 \rangle & \langle (S_{HH} + S_{VV})(S_{HH} - S_{VV})^{*} \rangle & 2\langle (S_{HH} + S_{VV}){S_{HV}}^{*} \rangle \\ \langle (S_{HH} - S_{VV})(S_{HH} + S_{VV})^{*} \rangle & \langle |S_{HH} - S_{VV}|^2 \rangle & \sqrt{2}\langle S_{HV}S_{VV}^{*} \rangle \\ 2\langle S_{HV}(S_{HH} + S_{VV})^{*} \rangle & 2\langle S_{HV}(S_{HH} - S_{VV})^{*} \rangle & 4\langle |S_{HV}|^2 \rangle \end{bmatrix} \quad (2)$$

Both, [*C*] and [*T*] matrices are by definition hermitian positive semi definite and have real non-negative eigenvalues but different eigenvectors. Both matrices are of rank 3 and contain equivalent information. Without ensemble averaging, both matrices are of rank 1 and characterize a deterministic scattering process. The sum of the diagonal elements (the trace) for both matrices is the same and represents the total power of the scattered wave.

1.3.2. Four-Component Decomposition

The complexity of scattering process makes extremely difficult the physical study of a given scatter through the direct analysis[*C*] or [*T*]. For this reason, polarimetric decomposition technique is used. Considering a vegetated medium with multilayered structure composed of branches, trunks and ground. Backscattering from vegetated terrain is typically mixture of several scattering mechanism such as surface scattering, which comes from the forest ground, volume scattering or multiple scattering from the canopy of the trees and double-bounce from ground-trunk. The contribution of this scattering mechanism depends on the frequency of the EM wave, incidence angle, structural properties of different tree species, environmental conditions, and moisture content of the ground and the canopy of the tree. Polarimetric decomposition model decomposes [*C*] or [*T*] matrix into three scattering mechanism such as surface scattering, double-bounce and volume scattering [12,29]. Yamaguchi *et al.* [29] proposed a four-component scattering model by adding a helix scattering term as a fourth component based on the coherency matrix for fully polarimetric SAR images. The coherency matrix is expanded into four sub matrices, which correspond to surface scattering, double-bounce scattering, volume scattering, and helix scattering mechanisms:

$$\langle [T] \rangle = f_s \langle [T] \rangle_{surface} + f_d \langle [T] \rangle_{double} + f_v \langle [T] \rangle_{volume} + f_h \langle [T] \rangle_{helix} \quad (3)$$

where f_s, f_d, f_v and f_h are the expansion coefficients to be evaluated, and $\langle [\boldsymbol{T}] \rangle_{\boldsymbol{surface}}$, $\langle [\boldsymbol{T}] \rangle_{\boldsymbol{double}}$, $\langle [\boldsymbol{T}] \rangle_{\boldsymbol{volume}}$ and $\langle [\boldsymbol{T}] \rangle_{\boldsymbol{helix}}$ are the scattering models for the surface, double-bounce, volume, and helix scatterings respectively.

The scattering powers P_s, P_d, P_v and P_h correspond to surface, double-bounce, volume and helix scattering power and are measured by the expansion coefficients f_s, f_d, f_v, f_h and the traces of the four sub matrices (Equation (3)). The polarimetric decomposition scattering powers are expressed as:

$$P_s = f_s(1 + |\beta|^2) \tag{4}$$

$$P_d = f_d(1 + |\alpha|^2) \tag{5}$$

$$P_v = f_v = 2T_{33} - 2P_h \tag{6}$$

$$P_h = f_h = 2|Im\langle(S_{HH} - S_{VV})S_{HV}^*\rangle| \tag{7}$$

The scattering powers P_s, P_d, P_v and P_h will be statistically compared with the forest GSV.

2. Study Area

Among the eleven forest territories used in Russia for the ALOS Kyoto and Carbon Initiative phase 3, led by JAXA Earth Observation Research Center (EORC), the three forest territories Shestakovsky, Chunsky and Primorsky were selected as for the investigation of polarimetric analysis (Figure 1). Each forest territory comprises a certain number of test areas, which are called forest compartments. These three territories belong to the southern taiga sub-zone of the boreal forest and belong to two Russian Siberian Federal Districts: Krasnoyarsk Kray and Irkutsk Oblast. Due to lack of multi-temporal SAR images over all the forest compartments, only one or two forest compartments of each test area was investigated in this study.

Figure 1. Forest compartments in Central Siberia including forest inventory and weather stations. The three forest territories (inside the blue rectangular box): Chunsky, Primorsky and Shestakovsky are only investigated in this study.

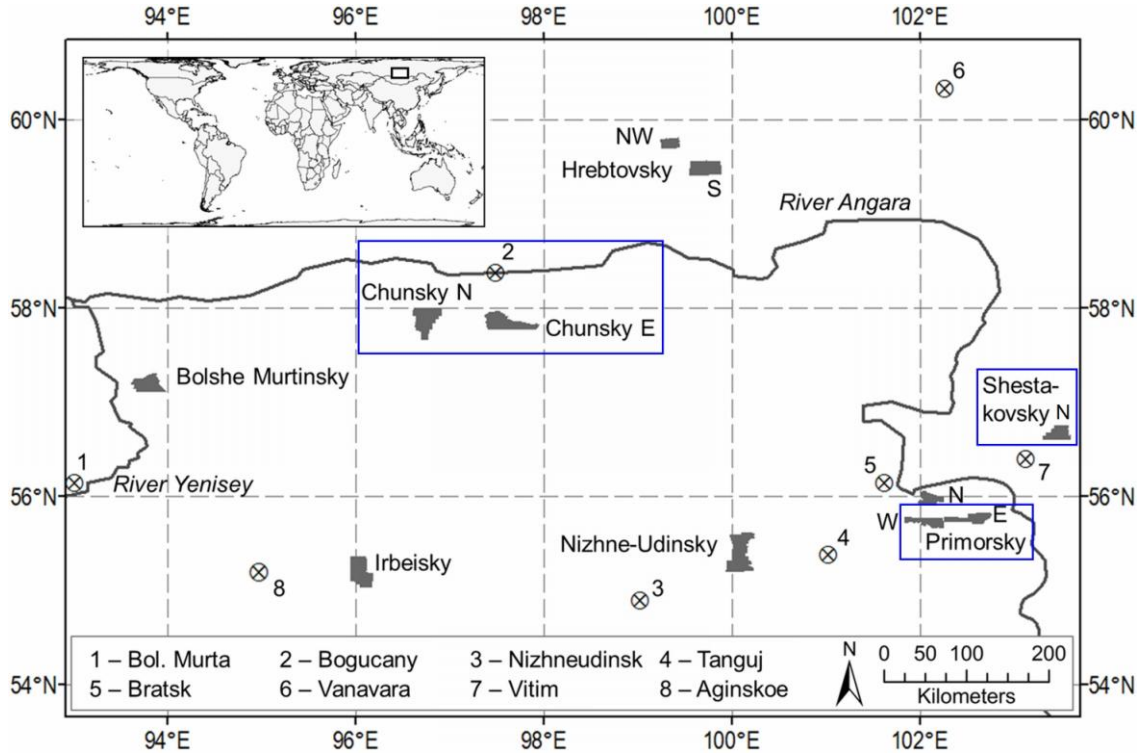

2.1. Shestakovsky

The Shestakovsky (center coordinates 104.45 °E, 56.67 °N) forest territory is 80 km north of the Bratsk Reservoir and 10 km west of the Llim River. Three compartments are included in this forest territory. The SAR image was acquired only over the northern compartment Shestakovsky-N. Its area is 146 km^2. The topography varies across Shestakovsky-N. High altitudes are found from the south-east corner to the north-west corner. The elevation ranges from 550 m to 700 m above the sea level (a.s.l). In south-east side of this test area 50% of the slopes are larger than 7 °. In the southern and western parts, the topography varies between 450 m and 550 m a.s.l. The standard deviation of the elevation is 60 m and 65% of areas have slopes up to 5 °. Detailed topographic information of all the investigated areas is illustrated in Figure 2.

Figure 2. Distribution of (**a**) slope angles and (**b**) topographic heights for the forest compartments in Siberia. The figure shows the mean (μ) and standard deviations (σ) of slope and topographic heights.

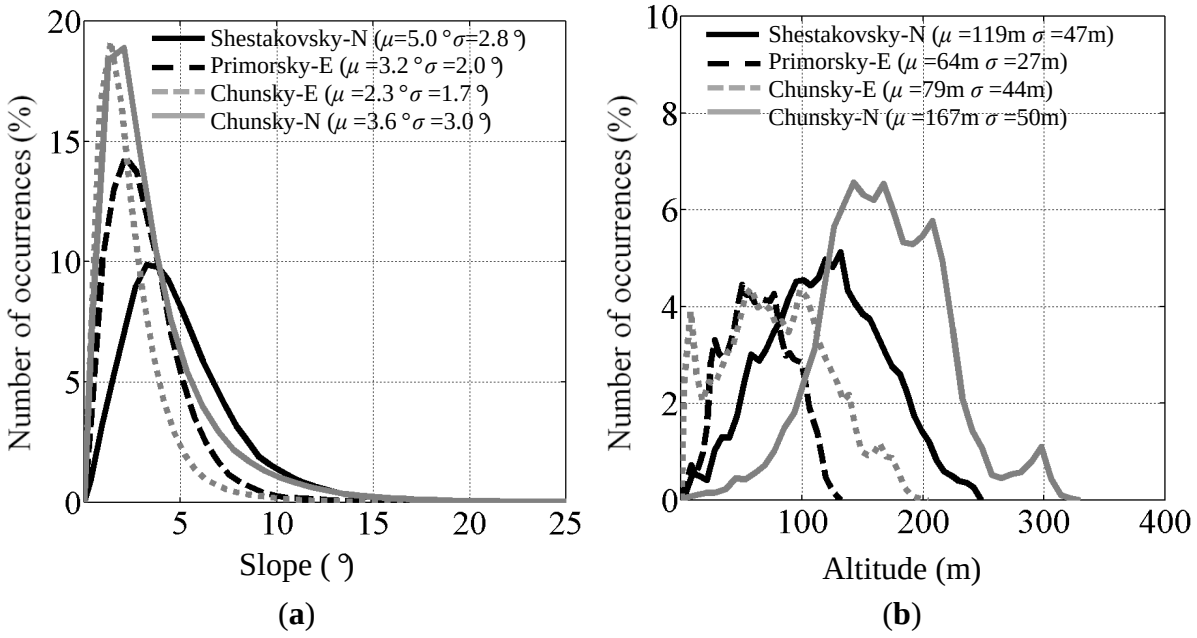

2.2. Primorsky

The Primorsky (center coordinates 102.20 °E 55.50 °N) forest territory is located on the southern bank of the Bratskove reservoir. The size of the easternmost forest compartment, Primorsky-E, is 326 km^2. In Primorsky-E, the topography is rather gentle with steep slopes along the rivers. The elevations range from 350 m to 400 m a.s.l. near the stream valleys and increase to 600m at the center of the compartment. Like in Shestakovsky-N, 65% of the area features slopes up to 5 °.

2.3. Chunsky

The forest territory Chunsky (center coordinates 96.40 °E, 57.40 °N) is located on the southern side of the river Angara. There are four forest compartments in this forest territory. In this paper, Chunsky-N and Chunsky-E are investigated. The size of the test areas is between 256 km^2 and 312 km^2. In

Chunsky-N and Chunsky-E the topography is mostly flat. The elevation in Chunsky-N is about 200 m a.s.l. in the southern part, where steep slopes are located along the river basins. In the northern part the elevation increases to 400 m a.s.l. In Chunsky-N, the topography is varying between 200 m and 250 m a.s.l. Few peaks reach altitudes of up to 340 m a.s.l. In 90% of the areas of Chunsky-N and Chunsky-E the slopes are smaller than 5 °.

3. Data Sets

3.1. Forest Inventory Data

The forest inventory data used in this study was originated from regular forest surveys in the framework of the Russian Forest Inventory Planning (FIP) and was part of an extensive Geographical Information System (GIS) database updated on 1998. The database consisted of forest stand boundary maps in digital form at stand level. A stand is the primary forest inventory unit where the borders were calculated from the aerial photographs. Each forest compartment comprises between 412 and 643 stands. Stand size is typically between 0.7 ha and 468 ha. About 90% of the total stands are below 60 ha. Only few stands are bigger than 100 ha. The forest stand size of both forest compartments in Chunsky is relatively larger than the stands in Shestakovsky-N and Primorsky-E. Stands are mostly labeled as natural stands. Remarkable for all the investigated areas is the large amount of forest stands that represent disturbed areas such as clear-cuts, fire scars, burned and harvest areas. This Siberian forest is commonly unmanaged.

The attributes of each stand are GSV (10 m^3/ha per class), relative stocking, age, height and diameter at breast height (dbh) of the dominant tree species, tree species composition *etc*. The GSV is the main parameter of interest in this study. The distributions of GSV for all the investigated areas are illustrated in Figure 3a. The GSV varies between 0 m^3/ha and approximately 400 m^3/ha for all the forest compartments. Clear-cuts and bogs are represented by a GSV of 0 m^3/ha. The histogram analysis of GSV for Shestakovsky-N and Primorsky-E in Figure 3a shows that a large number of stands contain dense forest. On the other hand, both in Chunsky-N and Chunsky-E, comparatively less dense forest stands are found. The greater number of stands with lower GSV has been noticed in Chunsky-N and Chunsky-E. This can be the significance of the different forest management practice performed in different test areas and also the intensive harvesting during past decades.

In both forest compartments, either very young or dense forests are dominant, whereas the intermediate growth stage between 50 m^3/ha and 100 m^3/ha is rarely found. According to Russian forest inventory standards the GSV accuracy should legally be between 12% and 15% (confidence interval 0.95), depending on economic value and age of the forest [33,42].

In the area of interest, the prevailing tree species are aspen (*Populus tremula*), birch (*Betula pendula*), fir (*Abies sibirica*), larch (*Larix dahurica* and *Larix sibirica*), pine (*Pinus sylvestris*), and spruce (*Picea sibirica*). The tree species composition for all the forest compartments is shown in Figure 3b. Birch and pine are the dominant species for all forest compartments. Cedar stands (*Pinus sibirica*) are found only in Shestakovsky-N. In all the forest compartments, young forests are dominated by deciduous forests, whereas conifers are predominant in mature forests. In general, at the Chunsky forest compartments the tree species composition is rather similar. However, in Shestakovsky-N and

Primorsky-E aspen is the dominant tree type at young forests, whereas birch dominates the young stands in Chunsky. The majority of the forest stands are natural stands with mixed tree species composition. Therefore, homogenous forest stands are rare in the test areas. The amount of stands with only single tree species varies between 4% and 11% for each of the forest compartments. Most of these homogenous stands comprise aspen, birch, pine, larch and also represent the dense forests. Only in Chunsky-E, aspen is not found. Tree species composition indicates the proportion of the species of the trees in a stand. The composition is listed separately for each tree species in a stand.

Figure 3. (**a**) Histogram of GSV distribution and (**b**) tree species composition for Shestakovsky-N, Primorsky-E,Chunsky-E and Chunsky-N (b).

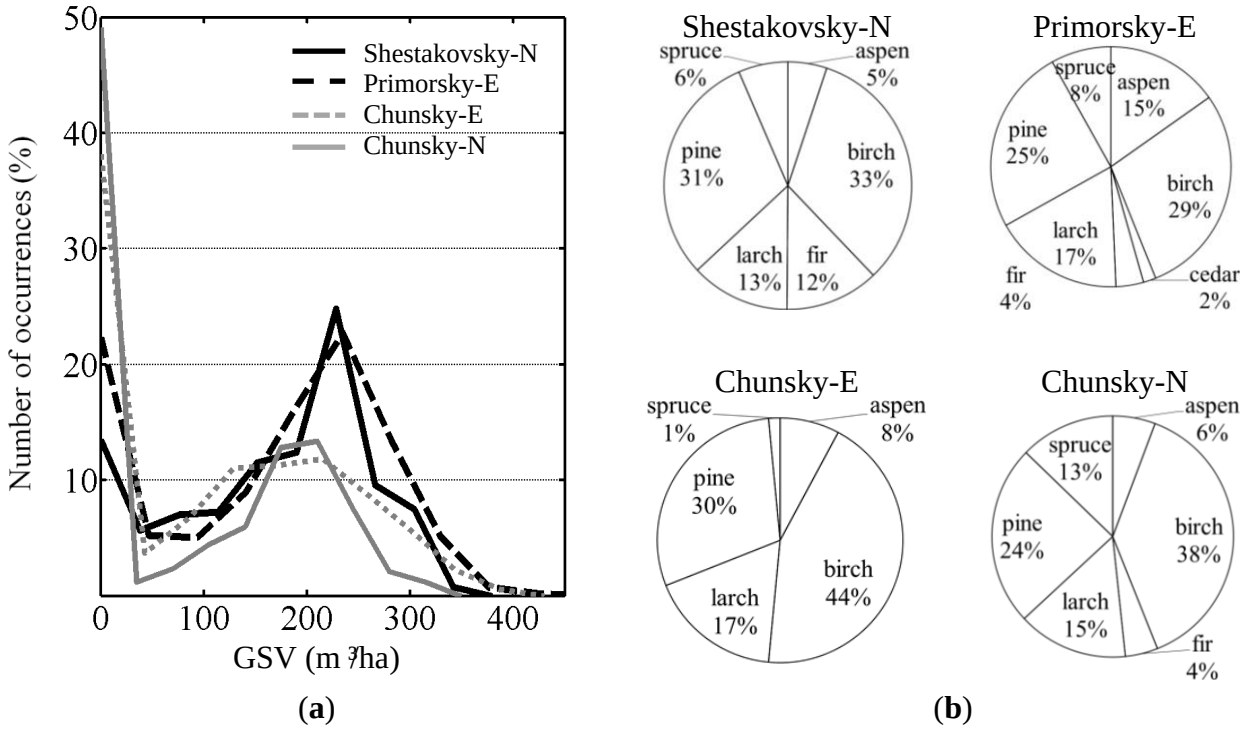

(**a**) (**b**)

3.2. Weather Data

The meteorological data was partly obtained from the German Weather Service (DWD). The other part was gathered from Weather Underground Website [43]. Two stations were placed near the Chunsky, two stations near the Primorsky and one station near the Shestakovsky. All the weather stations were located between 50 km and 100 km distance from the forest compartments. Daily measurements of temperature, precipitation, snow depth, wind speed, cloud cover, and dew point were available at all the stations. For Chunsky and Primorsky weather observations were recorded every 6 h. The station near Shestakovsky recorded every 12 h. A brief summary of the meteorological conditions is provided in Table 1.The values of the weather parameters reported in Table 1 represent the averages of the measurements of nearby weather stations. During winter, the temperatures were mostly below the freezing and snow accumulated on the ground while in summer the temperatures were above 0 ℃. Thus, in general, frozen conditions are assigned to winter and unfrozen conditions to summer acquisitions. Thaw is defined as when the minimum temperature was below freezing and maximum temperature was above freezing when snow is melting.

Table 1. Weather observations on the day of ALOS PALSAR L-band acquisitions for Siberian forests. "T" and "F" stands for the track and frame numbers for the PALSAR data. The time of overpass the satellite is between 23:30 h and 23:45 h (local time).

Forest Compartments	Acquisition Date	Temperature (℃)			Weather Conditions
		Min	Mean	Max	
Shestakovsky-N T-457 F-1130	21.05.2007	1	6	14	0.2 cm rain the day before (unfrozen, dry)
Shestakovsky-N T-457 F-1130	10.04.2009	−7	4	17	snowfall at 21:00 h last 2 days no snow; (thaw, wet)
Shestakovsky-N T-457 F-1130	26.05.2009	5	6	8	rainfall at 3:00 h and 21:00 h; last 2 days no rain (unfrozen, wet)
Primorsky-E T-459 F-1120	09.05.2007	4	7	13	light rain showers at 23:00 h and 00:00 h; last 1 week no rainfall (unfrozen, dry)
Primorsky-E T-459 F-1120	24.03.2007	−8	−3	−1	snowfall at 9:00 h last 20 days snowfall(frozen)
Primorsky-E T-460 F-1110	31.05.2009	6	17	22	last 3 days 1.6 cm rain (unfrozen, wet)
Chunsky-E T-467 F-1160	07.05.2007	−4	7	15	rain at 20:00 h; snowfall day before (thaw, wet)
Chunsky-E T-467 F-1160	19.09.2006	8	10	14	0.3 cm rain; 2 days before 1.1cm rained. (unfrozen, wet)
Chunsky-N T-468 F-1160	06.10.2006	−4	−3	1	snowfall; last day 3 cm snow; snow depth 16 cm (frozen)
Chunsky-N T-468 F-1160	13.04.2009	−12	−7	−1	snowfall; snow depth 20 cm (frozen)
Chunsky-N T-468 F-1160	21.08.2006	7	11	14	0.15 cm rain at 08:00 h: 2 cm rain last 4 days (unfrozen, wet)
Chunsky-N T-468 F-1160	24.05.2007	3	12	17	3 days before 0.5 cm rain (unfrozen, dry)

3.3. PALSAR Data

Fully polarimetric L-band SAR data have been acquired over the study areas by the Japanese Aerospace Exploration Agency (JAXA) using the Advanced Land Observing Satellite ALOS-PALSAR. The SAR data analyzed in this research are listed in the Table 1. Twelve SAR images were obtained from 2006 to 2009 at approximately 23:30 h (local time) at different meteorological conditions. All images were acquired on ascending orbit. According to JAXA's ALOS acquisition strategy, the polarimetric data were acquired once every two years with a look angle of 21.5 ° and twice every two years with a look angle of 23.1 °. Thus, it was not possible to gather a large multi-temporal dataset.

4. Methods

4.1. SAR Data Pre-Processing

Single look complex (SLC) level 1.1 PALSAR data were used for the investigations. First of all, the data was polarimetrically calibrated [44]. Afterwards, the coherency matrix [*T*] was formed. In this step, the data was multi-looked with 7 azimuths and 1 range looks and speckle filtered using 3 × 3 Lee Sigma filter [45]. The multi-looked factors result in approximately squared pixels. The Faraday rotation was calculated and eliminated [46].

The polarimetric SAR data were corrected for the impacts of azimuth slope. To compensate this slope affect, the polarization orientation angles (POA) were derived from the circular polarization algorithm [47], as shown in Equation (8):

$$\theta = \frac{1}{4}\left[\tan^{-1}\left(\frac{-2Re[T_{23}]}{-T_{22}+T_{33}}\right)\right] \tag{8}$$

where θ is the phase difference between the right-right and left-left circular polarizations. After the estimation of POA, a new rotated coherency matrix $T(\theta)$ was formed:

$$T(\theta) = [R_{3P(\theta)}][T][R_{3P(\theta)}]^{-1} \tag{9}$$

where $R_{3p}(\theta)$ is the unitary LOS rotation matrix.

$$[R_{3p}(\theta)] = \begin{bmatrix} 1 & 0 & 0 \\ 0 & \cos 2\theta & \sin 2\theta \\ 0 & -\sin 2\theta & \cos 2\theta \end{bmatrix} \tag{10}$$

The circular polarization algorithm was applied to all L-band data. Figure 4 illustrates one example for Shestakovsky-N. Figure 4a shows the POLSAR data with Pauli color coding (|HH−VV| for red, |HV| for green and |HH+VV| for blue). Buildings, bare surfaces, and areas with low vegetation are shown in the lower part of the image. The areas in upper part of the image are covered with forest of different tree species: aspen, birch, larch and pine. The POA map derived from the circular polarization is shown in Figure 4b. The POA varies between −25 ° and +25 °. The POA is noisier in forest areas, where much of the backscattered energy comes from the volume of the canopy. The areas with bare surfaces and buildings have meaningful orientation measurements. The SRTM DEM is shown in Figure 4c.

We applied the four-component decomposition to this new rotated coherency matrix $T(\theta)$ and calculated $P_h(\theta)$, $P_s(\theta)$,$P_d(\theta)$ and $P_v(\theta)$. Finally, the images were ortho-rectified using SRTM-3 DEM (Shuttle Radar Topography Mission-3 Digital Elevation Model) and orbit information. The pixel spacing of the geocoded images is 25 m × 25 m.

It is mentioned before that the data is speckle filtered using the 3 × 3 Lee Sigma filter. The impact of filter is demonstrated in Figure 5. The black polygons indicate the boundaries of forest stands. The result of the filtered image (Figure 5b) shows the positive effect of the filtering. Surface and volume scattering are smeared in the filtered image (Figure 5b). The dominant scattering properties have been preserved. Double-bounce, surface, and volume scattering are observed to produce peaks with less variance.

Figure 4. ALOS-PALASAR L-band data of Shestakovsky-N for illustration. (**a**) The Pauli RGB image. R = |HH − VV|, G = |HV| + |VH| and B = |HH + VV|. (**b**) The POA derived from circular polarization algorithm. (**c**) Digital Elevation Model (DEM) from SRTM-X.

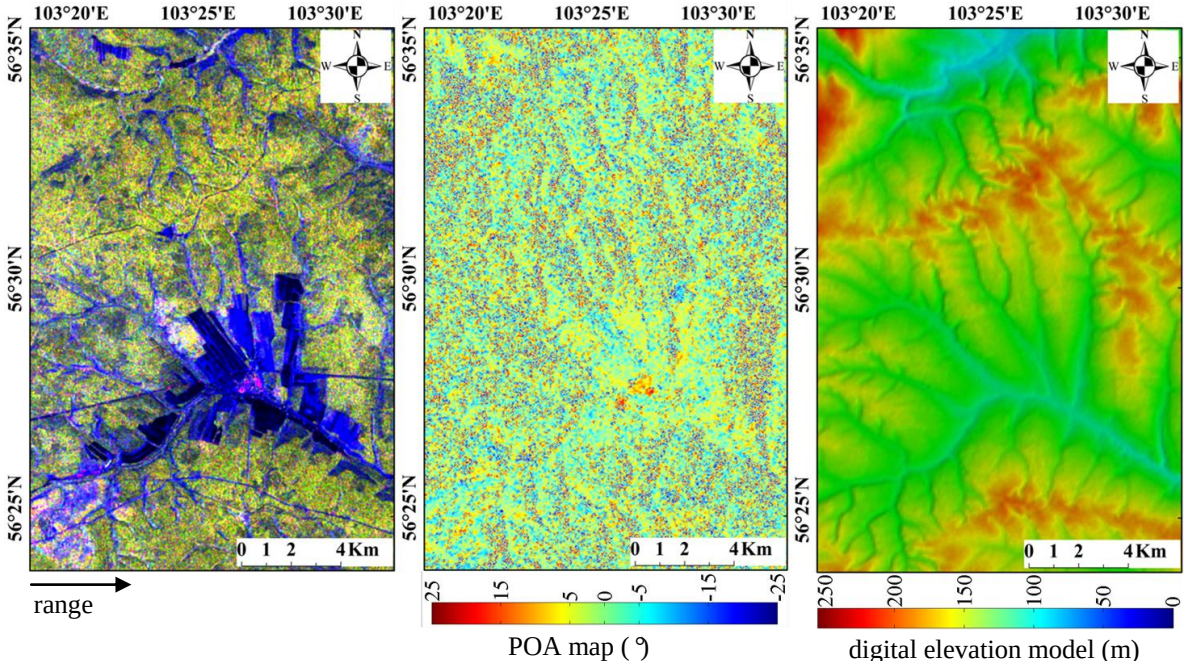

Figure 5. Distribution of decomposition powers (**a**) before and (**b**) after applying the 3 × 3 LEE filter. The red, green, and blue colors represent the double-bounce, volume, and surface scattering power respectively. The black polygons in insets indicate the boundaries of forest stands. Each scattering power is segmented into 40 samples.

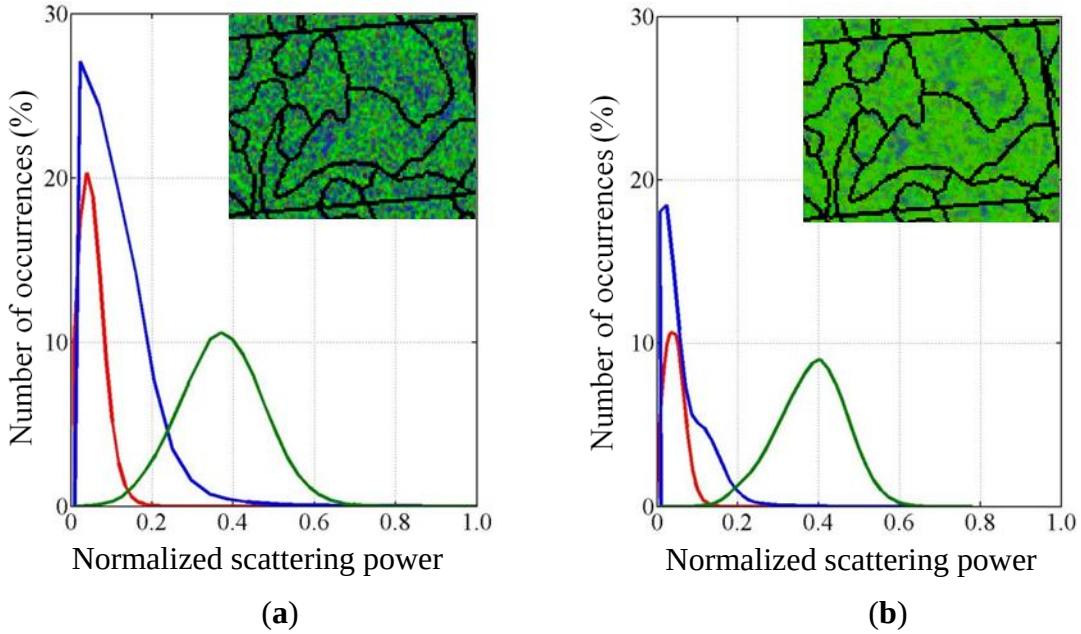

4.2. In-Situ *Data Pre-Processing*

To reduce the border effects and minimize the localization errors, the forest stands were buffered by 25 m and after that the stand-wise forest inventory data were converted to raster format and resampled to 25 m as used in the ortho-rectification of the SAR data. To limit the effect of speckle on the stand-wise polarimetric decomposition power measurements, we considered only stands larger than a given threshold. For each forest, compartments the threshold is set empirically depending on the number of stands left for further investigations. In Shestakovsky-N only stands larger than 2 ha (32 pixels) and in Primorsky-E, Chunsky-E and Chunsky-N the stands bigger than 5 ha was considered. [48–50] restricted their analysis for the retrieval of GSV from the SAR image to forest stands bigger than 2 ha.

Based on SAR data, the mean and standard deviations of decomposition power $P(\theta)$ have been computed for each stand. Because the stand size is up to 468 ha, the stand-wise mean are no longer sufficient to describe the underlying area. In this paper, stands size bigger than 60 ha (90th percentile of stand size) and stands with strong spatial heterogeneity of polarimetric decomposition powers, *i.e.*, strong differences in forest cover within a stand are excluded. The removal of heterogeneous stands was accomplished by means of standard deviation of polarimetric decomposition powers. The measured standard deviation of polarimetric decomposition powers for 2–10 ha stands are between 0.04 and 0.08. Therefore, a higher standard deviation indicates a very heterogeneous forest cover within the stand. From the histogram analysis of stand-wise standard deviation of polarimetric decomposition powers ($\sigma_{P(\theta)}$), a threshold of $\sigma_{P(\theta)} = 0.1$ is set for excluding heterogeneous forest stands. The stands with $\sigma_{P(\theta)} > 0.1$ are excluded. The number of remaining stands of each forest compartment used in this study is given in Table 2 where summary of the main characteristics of the each forest compartment is also reported.

Table 2. Forest stands summary statistics for all the forest compartments under investigations. The number within the bracket was provided in the forest inventory database.

	Shestakovsky-N	**Primorsky-E**	**Chunsky-E**	**Chunsky-N**
Area (km^2)	86 (146)	170 (326)	146 (256)	200 (312)
Number of Stands	234 (412)	405 (643)	320 (564)	302 (587)
Slope: min-mean-max (°)	0.8-5.0-13.2	0.9-3.2-12.0	0.5-2.3-9.6	0.6-3.6-10.0
Stands size: min-mean-max-stdv (ha)	2-22-60-12	5-28-60-13	5-25-60-15	5-30-60-12
GSV: min-mean-max-stdv (m^3/ha)	0-189-350-36	0-187-410-105	0-133-430-114	0-107-350-106

The outdated forest inventory data (from 1998) were updated using high resolution optical data regarding recent logging and other disturbances. The Multi-Purpose Satellite (KOMPSAT-2) from the Korea Aerospace Research Institute (KARI) data was used for this purpose. If any mismatch was found between optical images and ground-truth data, the stands were excluded.

Santoro and Cartus [51] introduced a following growth model for Siberian forests to overcome the time gap between this reference data set and ASAR data.

$$GSV_1 = 0.9867 \times GSV_{inv} + 5 \quad (11)$$

$$GSV_2 = 0.9867 \times GSV_1 + 5 \quad (12)$$

$$GSV_{up} = 0.9867 \times GSV_{n-1} + 5 \quad (13)$$

where GSV_{inv} is the original value from the forest inventory, GSV_1, GSV_2, GSV_{n-1} represent the yearly updated GSV and GSV_{up} defines the updated GSV. The authors assumed that for the region of Central Siberia, where the forest compartments are located, forests grow annually on average by 5 m^3/ha/yr. The updated GSV from the growth model has been done on a yearly basis using the value computed for the preceding year. We applied this growth model to the forest inventory. No significant difference has been observed for the trend between L-band ALOS PALSAR polarimetric decomposition powers and updated GSV. The proposed growth model does not consider for the different tree species and their growth rate, which are found to be different in Siberian forest where mixed forests are prevalent. Moreover, forest stand structure is very important parameter for the forest growing. GSV reaches higher levels for well managed forest stands. Therefore, it is not suitable to implement the growth model to the Siberian forests without precise knowledge of the growth of the individual tree species and stand structure change. Furthermore, development of growth model was not a topic of this study.

5. Results

5.1. Impact of Line of Sight (LOS) Rotation

Before applying the four-component decomposition powers to the ALOS PALASAR L-band data obtained from the Siberian forests to extract GSV information, the impact of line of sight rotation is investigated in this section. Yamaguchi *et al*. [52] published an approach of how the rotation of coherency matrix can be used to correct the POA. The effect of this correction is particularly observable in urban areas, if buildings are not orthogonal to the radar LOS. In this study, the investigation is carried on forest areas in Siberia. Figure 6 depicts the impact of applying the POA compensation to Yamaguchi four-component decomposition. The mean values and the standard deviations of polarimetric decomposition powers P_h, P_d, P_s, P_v, and $P_h(\theta)$, $P_d(\theta)$, $P_s(\theta)$, $P_v(\theta)$, have been computed for different slope classes. The mean values are shown as squares and the vertical bars represent the standard deviation of the mean decomposition powers of the stands within the slope classes. The mean GSV and their standard deviations of the corresponding slope classes are listed in Table 3. The mean GSV of all slope classes varies between 193 m^3/ha and 208 m^3/ha. The standard deviations range between 54 m^3/ha and 67 m^3/ha. The derived POA vary between −3.9° and +4.8° for all the investigated areas. The POA extracted from polarimetric data shows a high standard variation mainly due to the phase noise. The POA compensation results in a decrease of volume scattering and an increase of double-bounce and surface scattering. The helix scattering power remains unchanged because of its roll-invariant nature. The amount of decrease of volume scattering is equal to the amount of increase of double-bounce and surface scattering. For all slope classes, double-bounce and surface scattering power increase between 7% and 13%, whereas volume scattering power decreases between 13% and 25%. The POA estimated from the ALOS PALSAR L-band images acquired at frozen conditions is slightly sensitive to topography than the one derived from images acquired at unfrozen conditions.

The above investigation is carried out for dense forest. To demonstrate further the LOS rotation effect, the analyses are also performed for sparse forest where mean GSV is between 6 m^3/ha and 10 m^3/ha. For 0°–3° slope class, double-bounce and volume scattering increases and decreases

respectively between 4% and 7% while for high topography (11°–15° slope class) double-bounce and volume scattering increases and decreases respectively between 15% and 23%. The changes are much greater for high terrain areas. Therefore, LOS rotation has clear impact for topography under the sparse forest.

Figure 6. The mean normalized scattering power of the decomposition parameters (**a**) before and (**b**) after the rotation of coherency matrix for different slope classes. Red, green, blue, and black represent double-bounce, volume scattering, surface scattering, and helix scattering power respectively.

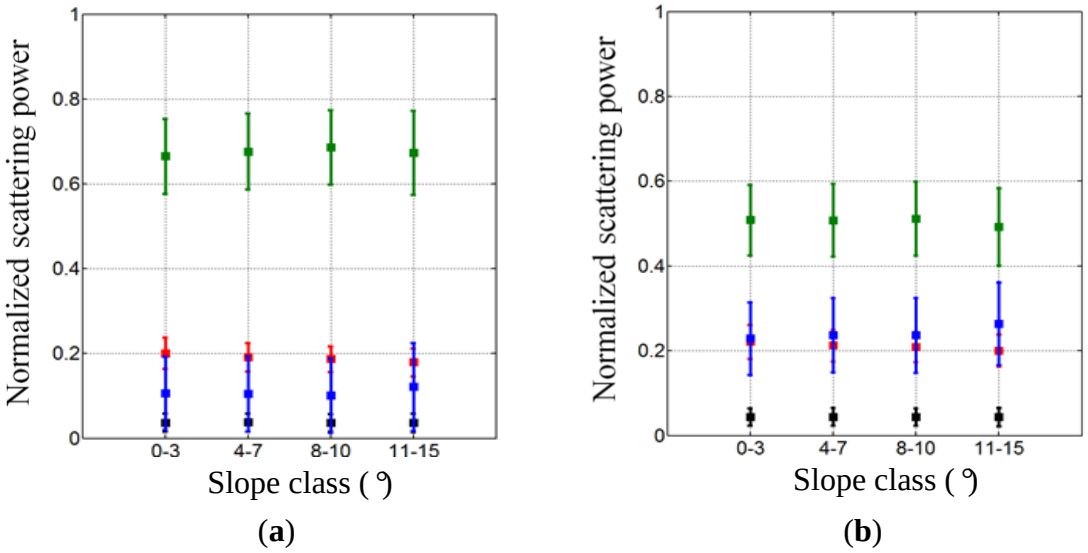

Table 3. Mean (μ) and standard deviation (σ) of GSV and polarization orientation angles (POA), derived by circular polarization algorithm for different slope classes.

Slope Class (°)	μ GSV (m^3/ha)	σ GSV(m^3/ha)	μ POA (°)	σ POA (°)
0–3	193	78	±3.9	2.3
4–7	208	78	±4.3	2.7
8–10	205	74	±4.5	2.9
11–15	202	87	±4.8	3.3

5.2. Growing Stock Volume and Polarimetric Decomposition Powers

The relationships between GSV and stand-wise polarimetric decomposition powers P_s (blue color), P_d (red color), and P_v (green color) are illustrated in Figure 7 for Shestakovsky-N, Primorsky-E, Chunsky-E and Chunsky-N. Helix scattering power is not shown here since it characterizes mainly artificial targets. The same colors for correspond scattering powers are also used in the remaining figures of this paper. All analyses in this research have been conducted on forest stand level. Therefore, the decomposition powers are measured by averaging all the pixels within each stand. In all cases, the stand-wise average of P_d, P_v increases and P_s decreases with the increasing of GSV. Considering the uniform distribution of both GSV and forest stands, the GSV is grouped into three

different stand sizes: 5–25 ha, 26–40 ha and 41–60 ha. Different range (2–20 ha, 21–40 ha and 41–60 ha) of stand size was used for Shestakovsky-N.

Figure 7. Relationship between GSV and polarimetric decomposition powers, derived without rotation of coherence matrix. Red, green, and blue represent the double-bounce scattering P_d, volume scattering P_v, and surface scattering P_s, power respectively. "n" represents the number of forest stands.

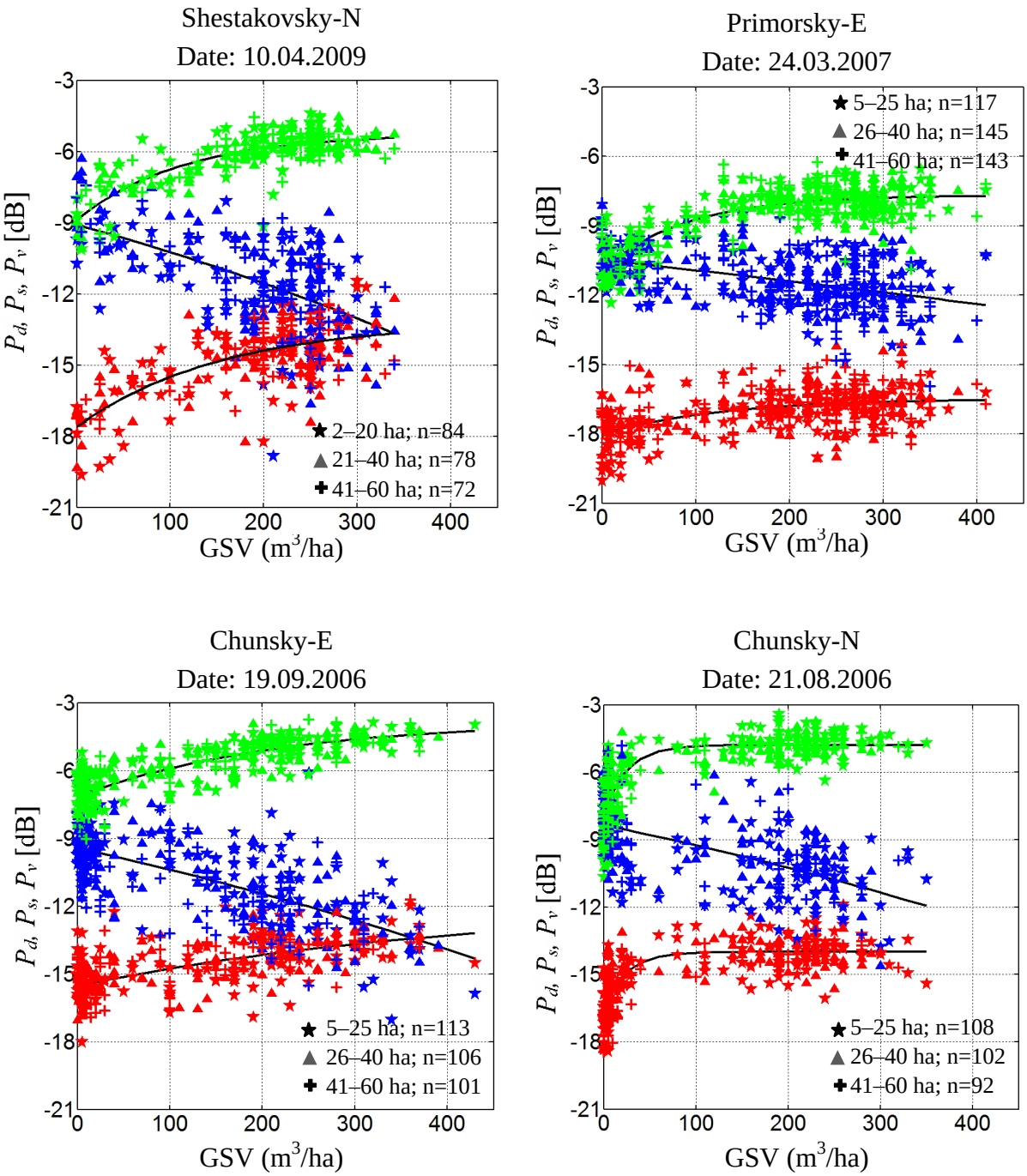

Figure 8. Relationship between GSV and polarimetric decomposition powers, derived with rotation of coherence matrix. Red, green, and blue represent the double-bounce scattering P_d, volume scattering P_v, and surface scattering P_s, power respectively.

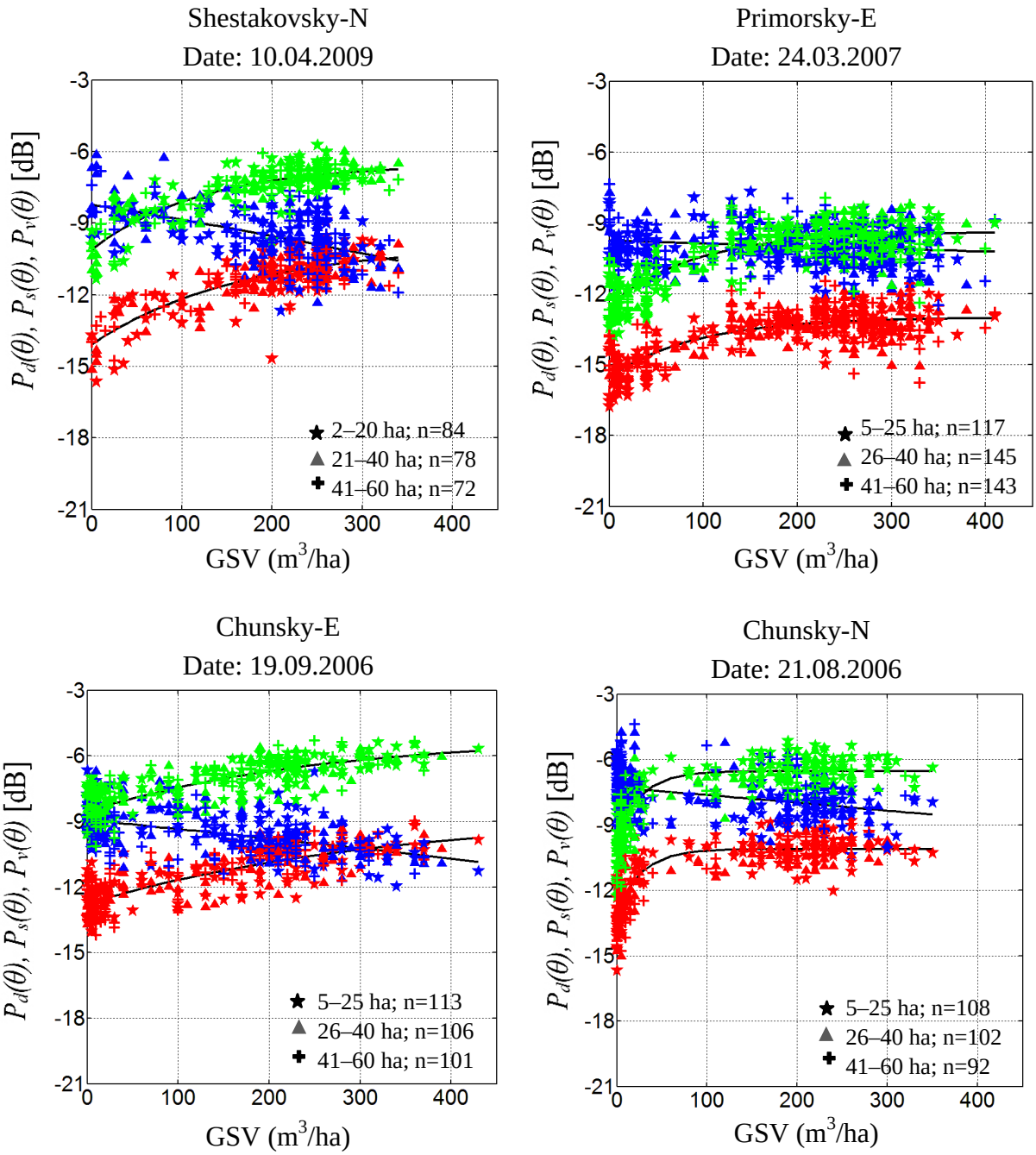

Similarly, Figure 8 shows the same trend for $P_s(\theta)$, $P_d(\theta)$, and $P_v(\theta)$. To allow a quantitative analysis between the GSV and polarimetric decomposition powers, Pearson's correlation coefficient (r) has been calculated for all plots. Pearson's correlation coefficients are reported in Table 4. The $P_d(\theta)$ correlation is significantly better than P_d for the entire forest compartments for all the acquisitions. On the other hand, the correlation between $P_s(\theta)$ and GSV decreases. Especially for all the acquisitions in Primorsky-E and for one acquisition (21 August 2006) in Chunsky-N, the $P_s(\theta)$ correlation declines noticeably compared to P_s The correlation between GSV and $P_v(\theta)$ as well as P_v

are almost the same. The p-values are less than 0.001 for the volume scattering, $P_v(\theta)$, double-bounce scattering, $P_d(\theta)$ and surface scattering, $P_s(\theta)$, which indicate the statistical significance of the correlation. Only some cases P-values are less than 0.002 for surface scattering, $P_s(\theta)$ (listed in Table 4 with "*"). The dependencies of polarimetric decomposition powers (P, $P(\theta)$) to the GSV of different stand sizes are investigated for all the forest compartments and no increase or decrease trend of correlation is observed as a function of stand size.

Table 4. Pearson's correlation coefficients for GSV-decomposition powers relationships, derived with and without rotation of coherency matrix. P_d, P_s, and P_v indicate double-bounce, surface and volume scattering power before the rotation of coherency matrix, whereas $P_d(\theta)$, $P_s(\theta)$ and $P_v(\theta)$ refer double-bounce, surface and volume scattering power after the rotation of coherency matrix.

Forest Compartments	Dates	P_d	$P_d(\theta)$	P_s	$P_s(\theta)$	P_v	$P_v(\theta)$
Shestakovsky-N	21.05.2007	0.26	0.70	−0.72	−0.61	0.70	0.73
Shestakovsky-N	10.04.2009	0.67	0.79	−0.56	−0.50	0.76	0.78
Shestakovsky-N	26.05.2009	0.31	0.71	−0.71	−0.61	0.75	0.76
Primorsky-E	09.05.2007	0.22	0.63	−0.54	−0.33*	0.66	0.66
Primorsky-E	24.03.2007	0.48	0.70	−0.43	−0.15*	0.74	0.74
Primorsky-E	31.05.2009	−0.15	0.46	−0.54	−0.37*	0.58	0.61
Chunsky-E	07.05.2007	0.38	0.70	−0.50	−0.53	0.76	0.76
Chunsky-E	19.09.2006	0.64	0.80	−0.67	−0.52	0.81	0.81
Chunsky-N	06.10.2006	0.16	0.56	−0.65	−0.60	0.65	0.67
Chunsky-N	13.04.2009	0.34	0.61	−0.64	−0.58	0.63	0.63
Chunsky-N	21.08.2006	0.61	0.77	−0.60	−0.36*	0.74	0.76
Chunsky-N	24.05.2007	0.49	0.69	−0.68	−0.62	0.72	0.73

*variable is significant at $0.001 < p < 0.002$.

From the Table 4 it can be seen that both, volume and double-bounce scattering power have positive correlation and surface scattering has negative correlation with GSV. According to these results, we can derive a relationship between the GSV and polarimetric decomposition powers. This can be expressed as:

$$GSV = f\left(\frac{P_d(\theta) \times P_v(\theta)}{P_s(\theta)}\right) \quad (14)$$

To simplify Equation (14), it is assumed that GSV is a function of volume-to-ground scattering ratio. For lower GSV or sparse forest, the numerator of Equation (14) is smaller and denominator is larger and *vice versa* for dense forest. Figure 9 shows the relationship between GSV and volume-to-ground scattering ratio for all the studied areas.

Figure 9. Regression between the ratio of double-bounce times volume scattering and surface scattering and GSV. Regression parameters are provided in Table 5.

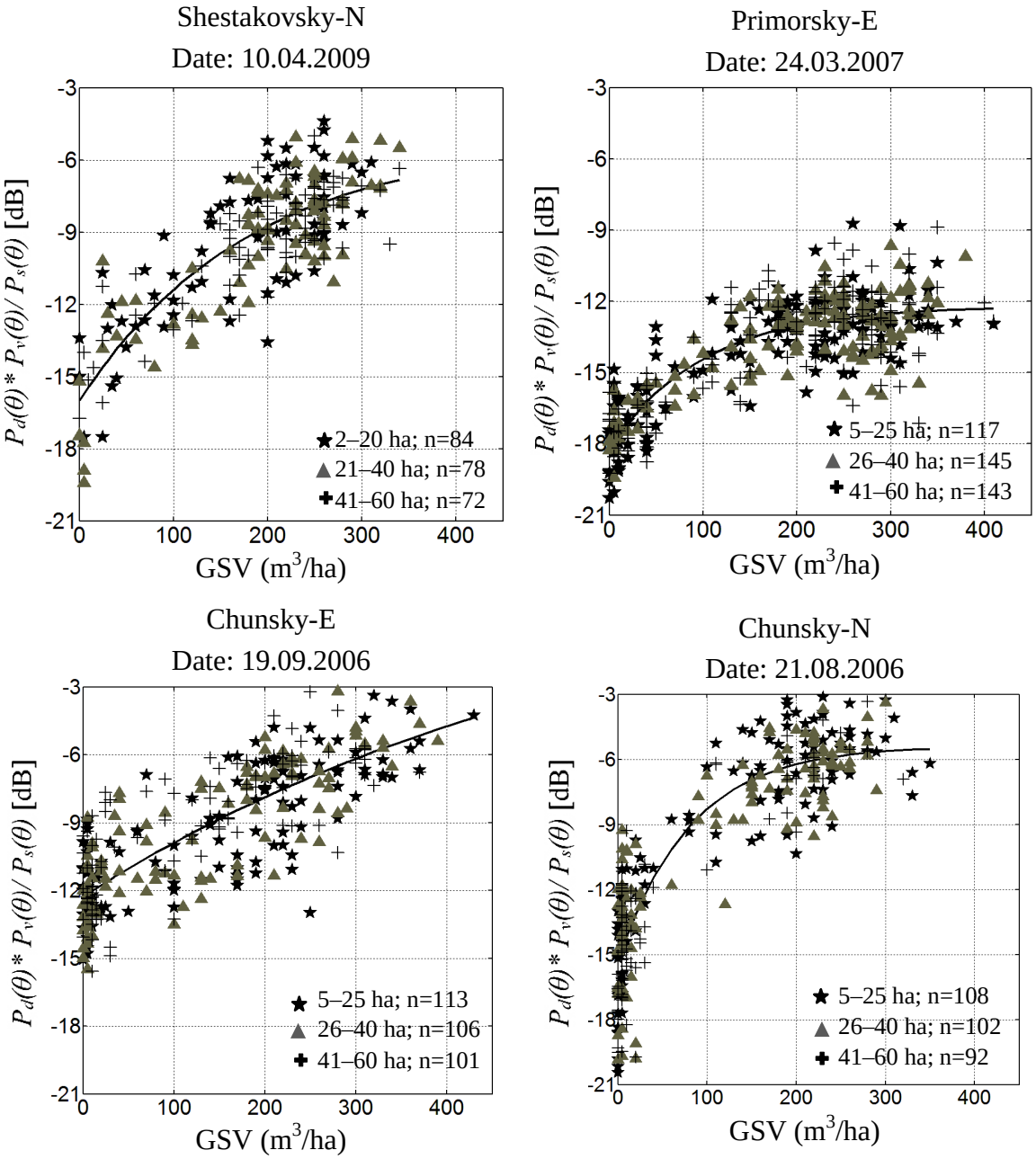

For the estimation it is necessary to have a model that as correctly as possible describes the relationship between the volume-to-ground scattering ratio and GSV. In previous studies [32,34,35,53–56], for space borne L-band coherence and backscatter indicated the exponential behavior with biomass related forest parameters. The scatter plots of Figure 9 are suggesting that the response of ratio of volume-to-ground scattering to GSV is nonlinear and also exhibits a clear increase of volume-to-ground scattering ratio with the increase of GSV. It is never observed to decrease with GSV over all the test areas. This nonlinear behavior can be well described by the model which was proposed by Wagner *et al.* [32], as shown in Equation (15):

$$\sigma^0(GSV) = \sigma_\infty + (\sigma_0 - \sigma_\infty) \times e^{-\frac{GSV}{GSV_\infty}} \quad (15)$$

where the model parameters,σ_0 represents the ratio of volume-to-ground scattering values at GSV = 0 m^3/ha (forest floor) and σ_- the saturated volume-to-ground scattering ratio for dense forest. GSV_- gives the rate of volume-to-ground scattering ratio increase with increasing GSV. The model parameters, Pearson's correlation coefficient r, the coefficient of determination R^2 and standard error of estimate are listed in Table 5. Based on the comparison of Table 4 with Table 5 it is said that the combination of the polarimetric decomposition powers by means of the ratio results increased Pearson's correlation coefficients.

Table 5. Estimated regression coefficients for decomposition powers and GSV. For better interpretation, a brief summary of weather conditions is provided also in this table. Detailed weather conditions are listed in Table 1.

Forest Compartments	Dates	σ_0(dB)	σ_- (dB)	GSV_- (m^3/ha)	r	R^2	SEE	Weather Conditions
Shestakovsky-N	21.05.2007	−12.6	−3.9	177	0.85	0.70	0.07	Unfrozen, dry
Shestakovsky-N	10.04.2009	−15.9	−5.1	190	0.80	0.68	0.06	Thaw, wet
Shestakovsky-N	26.05.2009	−11.8	−3.1	126	0.81	0.75	0.08	Unfrozen, wet
Primorsky-E	09.05.2007	−10.9	–6.0	114	0.74	0.64	0.08	Unfrozen, dry
Primorsky-E	24.03.2007	−18.2	−12.2	103	0.78	0.69	0.02	Frozen
Primorsky-E	31.05.2009	−10.2	−5.7	101	0.70	0.55	0.13	Unfrozen, wet
Chunsky-E	07.05.2007	−11.8	1.15	594	0.78	0.61	0.07	Thaw, wet
Chunsky-E	19.09.2006	−12.3	3.1	595	0.81	0.67	0.05	Unfrozen, wet
Chunsky-N	06.10.2006	−20.3	−12.2	128	0.84	0.79	0.05	Frozen
Chunsky-N	13.04.2009	−20.0	−12.3	126	0.90	0.82	0.05	Frozen
Chunsky-N	21.08.2006	−15.3	−5.4	82	0.87	0.81	0.07	Unfrozen, wet
Chunsky-N	24.05.2007	−15.2	−6.7	80	0.85	0.80	0.08	Unfrozen, dry

The parameter GSV_∞ varied in a wide range when fitting the model to the measurements at the forest compartments. The spread of the backscatter measurements was different depending on the test site. The ratio of volume-to-ground scattering increased almost linearly without apparent sign of saturation up to 430 m^3/ha in Chunsky-E whereas lowest saturation at 82 m^3/ha GSV was observed in Chunsky-N. This could be due to the spread of the ratio of volume-to-ground scattering measurements or lack of forest stands with GSV between 50 m^3/ha and 150 m^3/ha. The similar magnitude of $P_v(\theta)$ and $P_s(\theta)$ for high GSV can be one of the reason for lower saturation level which is illustrated in Figure 8 (Primorsky-E). Possible reason for the spread of volume-to-ground scattering ratio could be related either the forest structure or the accuracy of the measurements. Detailed investigations will be analyzed in future study.

5.3. Impact of Weather Conditions on Polarimetric Decomposition Powers

The consistencies of the polarimetric decomposition powers $P_s(\theta)$, $P_d(\theta)$, and $P_v(\theta)$ between multi-temporal acquisitions were investigated. The temporal consistency of the $P_d(\theta)$, and $P_v(\theta)$ was high with Pearson's correlation coefficients between 0.80 and 0.96. On the other hand, the temporal consistency of $P_s(\theta)$ was between 0.55 and 0.72.

Figure 10. Mean polarimetric decomposition powers for all acquisition dates. Red, green, and blue colors represent double-bounce, volume and surface scattering respectively for (**a**) sparse forest and (**b**) dense forest.

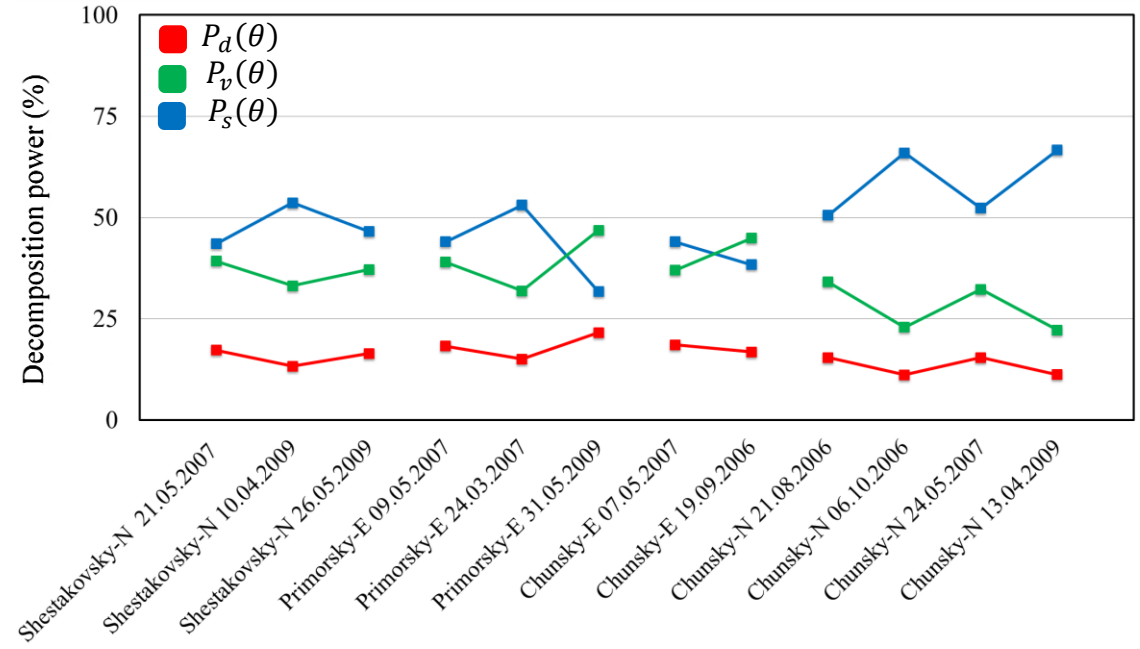

(**a**)

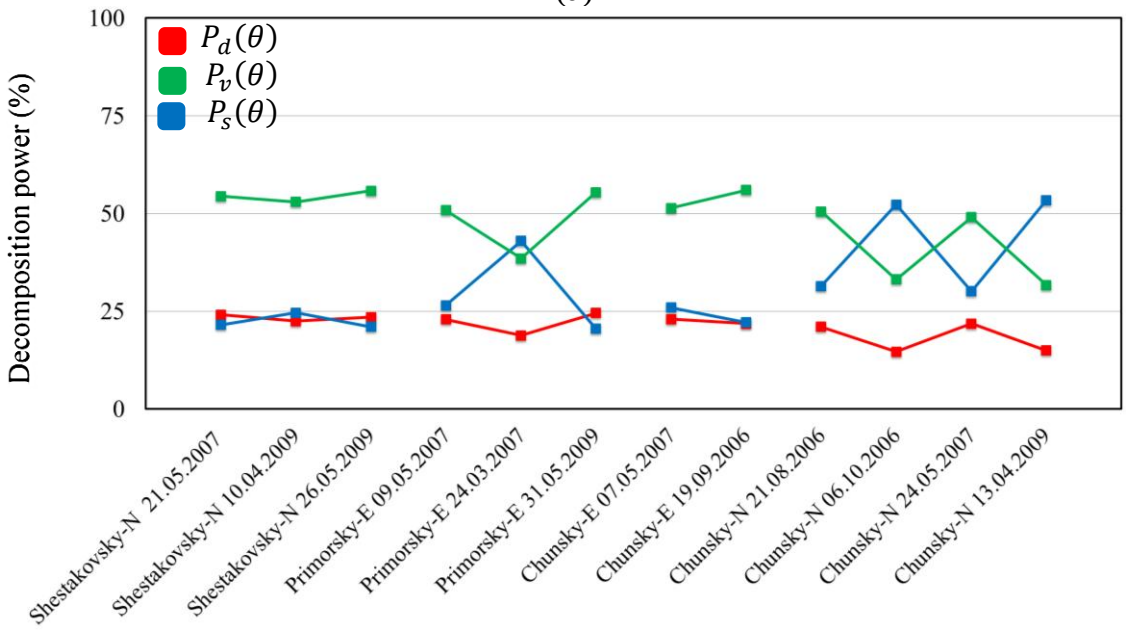

(**b**)

From Table 5 it has been evident that the estimated values ofσ_0 and σ_∞ are highly dependent on meteorological conditions, being higher at unfrozen conditions and lower at frozen or thawing conditions. At frozen conditions, the difference between the ground-to-volume scattering ratio from dense forest and sparse forest was 6–10 dB, where it was slightly lower under unfrozen conditions. A 5–8 dB difference between unfrozen and frozen condition was measured in sparse forest and dense forest Both the values of σ_0 and σ_∞ for each forest compartments correlate strongly with minimum temperature (see Table 1) of the L-band ALOS PALSAR acquisition (between 23:30 h and 23:45 h)

time. This may have caused considerable changes in dielectric constant, which as well decrease or increase the overall level of volume-to-ground scattering ratio in both forest floor and dense forest. The Pearson's correlation coefficients are greater than 0.90 for both cases.

To get an overview of how the contribution of polarimetric decomposition powers $P(\theta)$ change at different meteorological conditions, the normalized values of $P_s(\theta)$, $P_d(\theta)$, and $P_v(\theta)$ have been plotted for the corresponding acquisition dates. Figure 10a,b illustrates the mean values for sparse and dense forest. The sparse forests, where the forest canopy is characterized by large gaps, represent the stands with GSV from 0 to 20 m^3/ha. Dense forest comprises all stands with a GSV above 250 m^3/ha. By choosing these GSV ranges, a sufficient number of stands are available for each forest class. For the different forest compartments, the mean GSV for sparse forest varies between 6 m^3/ha and 10 m^3/ha. For dense forest, it varies between 273 m^3/ha and 300 m^3/ha.

In sparse forest, surface scattering $P_s(\theta)$ is more dominant than volume scattering, $P_v(\theta)$, and double-bounce $P_d(\theta)$. Exceptions are observed at unfrozen and rainy conditions where $P_v(\theta)$ is higher than $P_s(\theta)$ for sparse forest in Primorsky-E (31.05.2009) and in Chunsky-E (19.09.2006). During the frozen conditions $P_s(\theta)$ is more dominant than at unfrozen conditions. As $P_s(\theta)$ increases $P_d(\theta)$ and $P_v(\theta)$ decrease at frozen conditions.

In dense forest, $P_v(\theta)$ in general exceeds $P_s(\theta)$ or $P_d(\theta)$. At unfrozen conditions volume scattering and double-bounce scattering is stable in general. At frozen conditions, $P_v(\theta)$ is reduced and increased $P_s(\theta)$ was observed. $P_s(\theta)$ shows the highest scattering power for sparse forest at frozen conditions. $P_d(\theta)$ decreases slightly at frozen conditions.

5.4. Impact of Tree Species on Decomposition Powers

We have investigated the impact of tree species on $P(\theta)$ at three different meteorological conditions. All stands with a GSV above 150 m^3/ha have been selected. The four tree species aspen, birch, larch, and pine are considered. One problematic issue of this work is that pure stands (only one single species) are very rare. Therefore, the tree species that contributes at least 70% in stand were considered in this study. In Chunsky-N Aspen was not occurring. The mean and standard deviation of GSV of selected stands (>150 m^3/ha GSV) are given in Table 6.

Table 6. Mean (μ) and standard deviation (σ) of GSV for aspen, birch, larch, and pine in Siberian forests.

Forest Compartments	Aspen		Birch		Larch		Pine	
	μ (m^3/ha)	σ (m^3/ha)	μ (m^3/ha)	σ (m^3/ha)	μ (m^3/ha)	σ (m^3/ha)	μ (m^3/ha)	σ (m^3/ha)
Shestakovsky-N	267	28	201	23	242	37	259	46
Primorsky-E	290	48	205	26	239	53	278	46
Chunsky-E	266	55	212	24	198	17	302	38
Chunsky-N	—	—	172	13	225	30	250	52

The stand-wise mean values of $P_s(\theta)$, $P_d(\theta)$, and $P_v(\theta)$ for aspen, birch, larch and pine are depicted in Figure 11a–c for unfrozen, thawing, and frozen conditions respectively. At unfrozen and thawing conditions it has been observed (Figure 11a,b) that the scattering decomposition powers are not very

sensitive to tree species. Nevertheless, larch always shows the highest surface scattering. At thawing conditions (Figure 11b), double-bounce shows only 0.5 dB difference between deciduous trees and coniferous trees in Shestakovsky-N.

Figure 11. Mean decomposition powers over dense forests (GSV > 250 m^3/ha) separated by tree species at (**a**) unfrozen, (**b**) thawing and (**c**) frozen conditions. Red, green, and blue colors represent double-bounce, volume and surface scattering respectively.

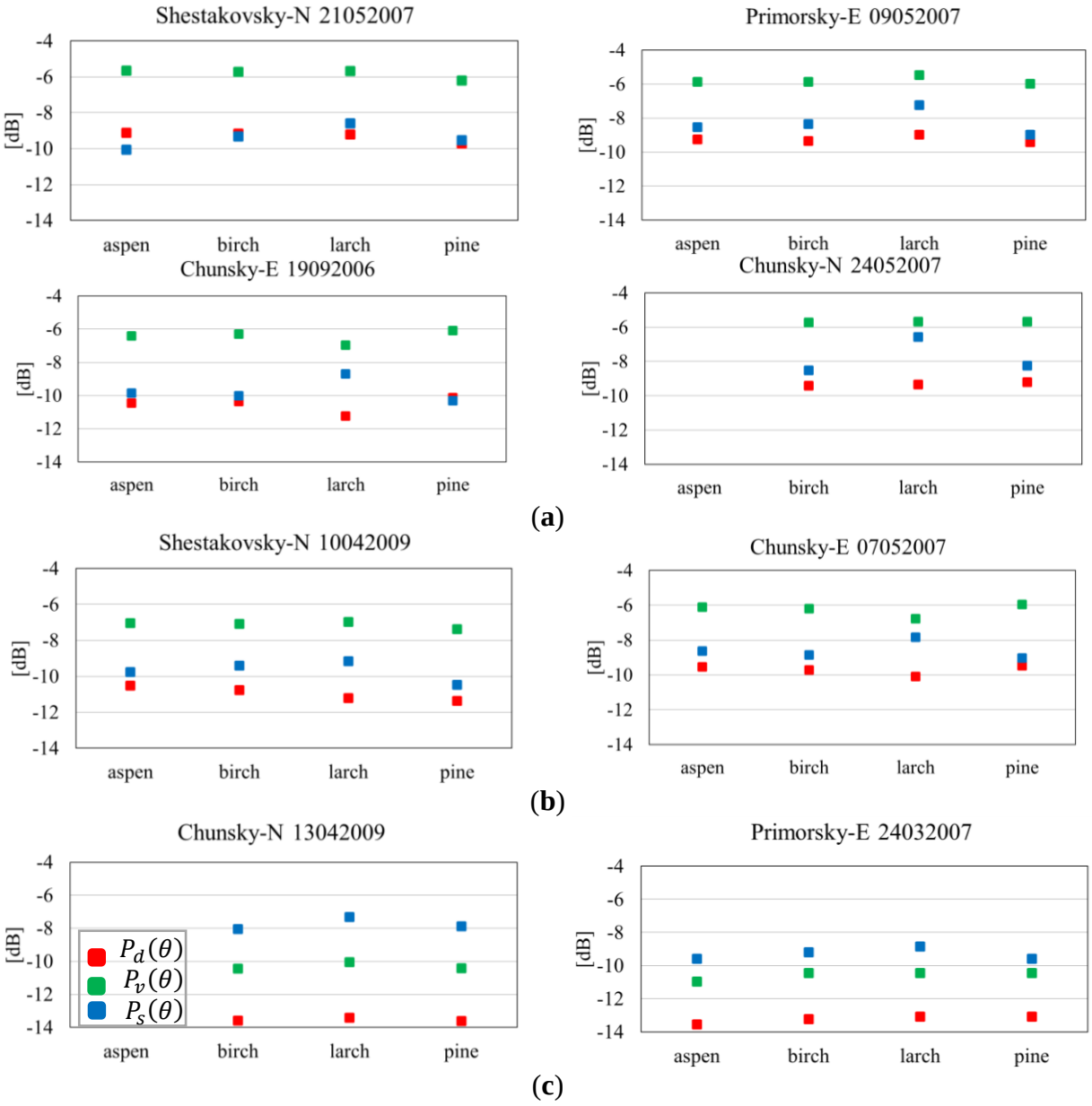

Two images in Chunsky-N and one image in Primorsky-E were acquired at frozen conditions (Figure 11c). $P_s(\theta)$ is higher than $P_v(\theta)$ at both forest compartments, $P_d(\theta)$ has the lowest contribution. Compared to unfrozen conditions, $P_v(\theta)$ and $P_d(\theta)$ are clearly reduced. During frozen conditions, the impact of the tree species on $P(\theta)$ is even smaller than at unfrozen conditions.

6. Discussions

6.1. Growing Stock Volume Estimation Using Polarimetric Information

In the Table 4 it is demonstrated that both, P and $P(\theta)$ show the similar direction of correlation with GSV. A high positive correlation for the volume scattering (r = 0.81; p-value < 0.001), a high positive correlation for the double-bounce scattering (r = 0.80; p-value < 0.001), and a high negative correlation for the surface scattering (r = −0.72; p-value < 0.001) have been observed for $P(\theta)$. The physical explanations for the observed relationships are (i) at low GSV there are many gaps in the canopy which increase the surface scattering; (ii) as the vegetation grows the canopy covers most of the ground which increases the volume scattering and decreases the surface scattering; (iii) the growth of the tree trunk increases the double-bounce scattering power.

Kobayashi *et al*. [28] applied Yamaguchi's four-component decomposition scheme to ALOS PALSAR L-band data to compare the decomposition powers with the forest parameters tree height, tree diameter, and stand volume in tropical forest. The authors showed that surface and volume scattering powers are slightly better positively correlated with the forest parameters after the rotation of coherency matrix. The surface scattering was negatively correlated and volume scattering was positively correlated with forest parameters. They found that there was no correlation between double-bounce and forest parameters. This could be due to the vestigial canopy effects in tropical forest. Different direction of correlation between GSV and decomposition power has been observed by Goncalves *et al*. [27]. They used airborne L-band SAR data to apply the Freeman-Durden decomposition [12] and showed that all the decomposition scattering powers were positively correlated with the stem volume of a tropical forest.

In our work, the rotation of the coherency matrix resulted in increased correlation between $P_d(\theta)$ and GSV in all study areas. Regarding the other polarimetric parameters, the rotation of the coherency matrix had almost no impact. This could be due to the fact that at L-band the penetration of the wave through the canopy might not be sufficient, resulting in noisy POAs in forested areas [47]. The authors investigated the POA measurements by applying JPL AIRSAR C-, L- and P-band data over the forest in Freiburg, Germany on 15 June 2001. They found that P-band data has deeper penetration than the C- and L-band in the heavy forested areas. Thus, the POA cannot be estimated accurately with ALOS PALSAR L-band in dense forest areas with varying topography. Further support to our assumptions was found in Li *et al*. [57]. The authors investigated that it is difficult to estimate accurate topography POA over vegetated terrain using L-band POLSAR data.

Goncalves *et al*. [27] set up a model by using multi-linear regression model of several incoherent and coherent attributes including volume scattering power of Freeman-Durden decomposition [12]. They showed that the GSV can be retrieved up to 308 m^3/ha. In this study, the high correlation coefficients for double-bounce and volume scattering provide the possibility to estimate the GSV. Despite the considerable effects of meteorological (unfrozen/frozen/thawing conditions) and environmental (snow properties) conditions, the temporal consistency of the $P_d(\theta)$ and $P_v(\theta)$ is high. This stability indicate the degree to which $P_d(\theta)$ and $P_v(\theta)$ change consistently that may be related to the robustness of using $P_d(\theta)$ and $P_v(\theta)$ to characterize GSV. Since the correlation for the surface scattering power is not consistent and strong enough for all the forest compartments, it should not be

considered for the GSV estimation. The inconsistent behavior could be due to (i) moisture effects and heterogeneity of dielectric properties due to the larger test sites; (ii) growth of small trees or forest understories; (iii) potential differences between forest inventory data from 1998 and the GSV at the time of the SAR acquisition; and (iv) potential inaccuracies of the forest inventory data.

The correlation between polarimetric decomposition parameters and GSV is improved (r varies between 0.70 and 0.90, p-value < 0.001) if volume-to-ground scattering ratio, *i.e.*, the ratio of $P_d(\theta)$ times $P_v(\theta)$ and $P_s(\theta)$ is used instead of individual polarimetric decomposition powers. The idea has been developed quantitatively using the two layer approach of surface and volume scattering in forest. When volume-to-ground scattering ratio is small, GSV is low and when volume-to-ground scattering ratio is large, GSV is high. The relations shown in Figure 9 and Table 5 indicate that the sensitivity of the volume-to-ground scattering ratio for GSV is increased and a large dynamic range is observed at all forest compartments. The spread in the data can depend on the spatial distribution of trees, canopy architecture, canopy moisture content, soil roughness and moisture.

The only exception has been found for the image acquired on 31 May 2009 at Primorsky-E. Medium Pearson's correlation coefficients $r < 0.61$ for the polarimetric decomposition powers, $P(\theta)$ and a relatively lower coefficient of determination $R^2 = 0.55$ for volume-to-ground scattering ratio has been observed. This could be due to a heavy impact of weather conditions. According to the weather data records (see Table 1) it didn't rain on the day of the SAR acquisition; however moderate rain (16 mm) was observed during the past three days before the acquisition.

6.2. Impact of Weather Conditions

The contributions of decomposition scattering powers depend on the environmental conditions at the time of acquisition. In sparse and dense forests, the behavior of surface scattering power and volume scattering power are opposed. At all the forest compartments, surface scattering power is dominant in sparse forest at unfrozen and dry conditions, while in dense forest the volume scattering power is dominant.

At unfrozen and wet conditions, the volume scattering is higher than the surface scattering in sparse forests. This could be due to the increased moisture content of the canopy resulting in decreased penetration. Therefore, the ground contribution is decreased. Under these circumstances, the volume scattering power can be as high as for dense forest. The higher dielectric constant of water under unfrozen and wet conditions makes the surface smoother and increase double-bounce scattering.

At frozen conditions, the surface scattering power is higher than the volume scattering power in dense forest. The differences between the contributions of scattering power from sparse and dense forests are nearly the same. In winter, canopies are frozen. Thus, the transmitted electromagnetic wave penetrates deeper into the canopy and a great amount of backscatter comes from the ground and the contribution of double-bounce and volume scattering decreases. The contribution of double-bounce is higher in dense forest than in sparse forest. This could be due to a large number of tree trunks within a radar resolution cell. Though the impact of snow is not thoroughly investigated, it is assumed that at L-band the impact of dry snow can be neglected.

Although several studies have shown the importance of the double-bounce scattering mechanism at L-band [58,59] but in this work, the double-bounce contribution is in general smaller than the volume

and surface scattering power. If the forest floor is smooth, ground-trunk interactions can significantly contribute to the total backscatter. However, in the forest many factors slope, dead wood, understories, *etc*. influence this kind of scattering mechanism. In Siberian forests, the floor often exhibits small bushes and trees, which can reduce the double-bounce scattering power. Double-bounce is also reduced, if the angle between trunk and ground surface is not equal to 90 degrees. This occurs in areas with pronounced topography and if the trunks are tilted. Further support to the assumption was reported by Pulliainen *et al*. [60], and Ranson and Sun [61]. They found the double-bounce term in boreal forests is negligible because of rough surface ground and strong attenuation in coniferous and broadleaf types of forest. Baker and Luckman [25] investigated the importance of double-bounce, surface and volume scattering in boreal forests with L-band EMISAR airborne sensor. The authors showed the dominance of volume scattering relative to the double-bounce scattering.

6.3. Impact of Tree Species

The geometrical properties of trees (e.g., crown shape, alignment of tree components) and environmental conditions (undergrowth, water consumption, interception, wind susceptibility, *etc*.) affect the polarimetric decomposition scattering composition. In this paper, the impact of polarimetric decomposition powers for aspen, birch, larch, and pine have been investigated at three different meteorological conditions: unfrozen (dry and wet), thawing and frozen.

Spatiotemporal variability of environmental conditions during the growing season (precipitation, soil moisture change, growth, *etc*.) result in increased spread (inter and intra species) variance of decomposition powers. At unfrozen conditions, the impact is increased in particular for larch. In Chunsky-N larch differs from other tree species by +2dB surface scattering power at unfrozen conditions. At the other sites the same behavior is observed, however the difference is slightly smaller than +2dB.The double-bounce and volume scattering power for larch was also differed by −1.5 dB and −1.2 dB respectively from other tree species in Chunsky-E.

Pine is conifer tree while aspen, birch and larch are deciduous and deciduous conifer respectively and have no leaves and needles during the early spring or late autumn when the ALOS PALSAR L-band images are acquired. During the leave-off periods because of the canopy transparency the attenuation of the electromagnetic wave decreases resulting in decrease of volume scattering and hence also increases of double-bounce and surface scattering. In Figure 11a, among the deciduous trees only larch shows higher surface scattering power than others. Moreover, larch shows (not illustrates in this Figure) the similar behavior *i.e*., higher surface scattering power for the image acquired at summer season (21 August 2006) in Chunsky-N. No difference of polarimetric decomposition powers between aspen and birch are observed. Therefore, the impact of larch cannot be due to the effect of seasonality but rather the structure of the tree.

The higher surface scattering power from larch forest can indicate that the canopy are more transparent to the electromagnetic wave and a large part of radar backscatter power comes from the ground. This could be due to the different canopy structures, different needles arrangement, less dense canopy. Moreover, there could be fewer understories in the larch forest stands and surface is smoother. Watanabe *et al*. [26] investigated the contributions of polarimetric coherence, double-bounce, surface and volume scattering power for spruce, fir, and larch forest in cool-temperate forest in northern Japan.

The results showed higher coherence value and surface scattering powers for larch forest. However, the physical significance of observed results is not discussed.

At frozen conditions, the impact of tree species on polarimetric decomposition power is very low and all tree species follow the same trend, no noticeable deviations occur. Because of the frozen canopy, geometric properties of tree species are of less importance. Therefore, the structural differences between the tree species cannot be distinguished. The species related shape and structure of the canopy have less impact on the polarimetric decomposition powers. Moreover, due to freezing the dielectric constant of the trees is reduced [62] and the forest ground is more exposed. This results in decreased attenuation and higher ground contribution. Thus, the amount of scattering within the canopy is decreased [63,64].

7. Conclusions

This paper considers several aspects for the possibility of GSV estimation in boreal forest at stand level using polarimetric information. Four forest compartments located in Central Siberia have been considered for the investigation. The four-component power decomposition method has been applied to the L-band ALOS PALSAR fully polarimetric data to compare the decomposition powers to the GSV and the impact of different meteorological conditions. The dependence of the decomposition powers on the tree species was also investigated. The main results of the study are as follows:

1. Double-bounce and volume scattering powers show significant correlation with growing stock volume. The correlation between GSV and surface scattering is found to be inconsistent.
2. The importance of the LOS rotation is demonstrated, as the correlation between double-bounce scattering power and GSV could be significantly improved.
3. The correlation between polarimetric decomposition parameters and GSV is enhanced if the ratio of volume-to-ground scattering, which is the ratio of volume scattering times double-bounce and surface scattering, is used instead of considering polarimetric decomposition powers separately. The volume-to-ground scattering ratio shows a high sensitivity to GSV. A relatively higher dynamic range is observed for all the investigated areas in Siberia.
4. The contribution of decomposition powers over the sparse and dense forest depends on the meteorological conditions. At unfrozen conditions, surface scattering is dominant in sparse forests while in dense forests volume scattering is dominant. During thawing conditions, volume scattering in sparse forests is increased. The scenario is totally different at frozen conditions for dense forest, where the surface scattering power is higher than the volume scattering power.
5. The stands dominated by larch species show higher surface scattering power than other tree species. Larch differs from aspen, birch and pine by +2 dB surface scattering power at unfrozen conditions. The double-bounce and volume scattering power for larch was also differed by −1.5 dB and −1.2 dB respectively. At frozen conditions, the impact of tree species on polarimetric decomposition powers is observed to be very small.

GSV estimation based on polarimetric data does not require multi-temporal data, as required for POLINSAR techniques. Furthermore, thanks to PALSAR polarimetric L-band data are already available for many areas on the globe, while suited POLINSAR datasets are still missing.

Acknowledgments

This work has been undertaken [in part] within the framework of the JAXA Kyoto and Carbon Initiative. ALOS PALSAR data have been provided by JAXA EORC. The KOMPSAT-2 data were delivered by the European Space Agency (ESA). The authors would like to thank the reviewers for their valuable comments and recommendations. This research work was done under the project TH 1435/2-1 funded by the DFG-Deutsche Forschungsgemeinschaft, Germany. The authors gratefully acknowledge the DFG.

Conflicts of Interest

The authors declare no conflict of interest.

References

1. Nilsson, S.; Shivdenko, A. *Is Sustainable Development of the Russian Forest Sector Possible?* IUFRO Occasional Paper No. 11 ISSN 1024–414X; IUFRO Secretariat: Vienna, Austria, 1998; p. 76.
2. Nilsson, S.; Shivdenko, A.; Stolbovoi, V.; Gluck, M.; Jonas, M.; Obersteiner, M. *Full Carbon Account for Russia*; International Institute for Applied System Analysis (IIASA): Vienna, Austria, 2000.
3. Le Toan, T.; Beaudoin, A.; Riom, J.; Guyon, D. Relating forest biomass to SAR data. *IEEE Trans. Geosci. Remote Sens.* **1992**, *30*, 403–411.
4. Luckman, A.; Baker, J.; Kuplich, T.M.; Yanasse, C.D.C.F.; Frery, A.C. A study of the relationship between radar backscatter and regenerating tropical forest biomass for space borne SAR instruments. *Remote Sens. Environ.* **1997**, *60*, 1–13.
5. Hoekman, D.H.; Quiñones, M.J. Land cover type and biomass classification using AIRSAR data for evaluation of monitoring scenarios in the Colombian Amazon. *IEEE Trans. Geosci. Remote Sens.* **2000**, *38*, 685–696.
6. Santoro, M.; Shvidenko, A.; McCallum, I.; Askne, J.; Schmullius, C. Properties of ERS-1/2 coherence in the Siberian boreal forest and implications for stem volume retrieval. *Remote Sens. Environ.* **2007**, *106*, 154–172.
7. Lee, J.-S.; Pottier, E. *Polarimetric Radar Imaging—From Basics to Applications*; CRC Press, Taylor & Francis Group: Boca Raton, FL, USA, 2009.
8. Van Zyl, J.J. Unsupervised classification of scattering behavior using radar polarimetry data. *IEEE Trans. Geosci. Remote Sens.* **1989**, *27*, 36–45.
9. Krogager, E. New decomposition of the radar target scattering matrix. *Electron. Lett.* **1990**, *26*, 1525–1527.
10. Cloude, S.R.; Pottier, E. A review of target decomposition theorems in radar polarimetry. *IEEE Trans. Geosci. Remote Sens.***1996**, *34*, 498–518.
11. Krogager, E.; Madsen, S.N. Comparison of Various Decompositions for Analysis, Interpretation and Classification of Polarimetric SAR Images. In Proceedings of European Conference on Synthetic Aperture Radar (EUSAR'96), Königswinter, Germany, 26–28 March 1996.

12. Freeman, A.; Durden, S.L. A three-component scattering model for polarimetric SAR data. *IEEE Trans. Geosci. Remote Sens.* **1998**, *36*, 963–973.
13. Cloude, S.R.; Pottier, E. An entropy based classification scheme for land applications of polarimetric SAR. *IEEE Trans. Geosci. Remote Sens.* **1997**, *35*, 68–78.
14. Ito, Y.; Omatu, S. Polarimetric SAR data classification using competitive neural networks. *Int. J. Remote Sens.* **1998**, *19*, 2665–2684.
15. Hellmann, M. Classification of Fully Polarimetric SAR-Data for Cartographic Applications. Ph.D. Thesis, TU Dresden, Dresden, Germany, 14 April 2000.
16. Lee, J.S.; Grunes, M.R.; Pottier, E.; Ferro-Famil, L. Segmentation of Polarimetric SAR Images. In Proceedings of IEEE International Symposium Geoscience and Remote Sensing (IGARSS'01), Sydney, Australia, 9–13 July 2001.
17. Schuler, D.L.; Lee, J.S.; Kasilingam, D.; Nesti, G. Surface roughness and slope measurements using polarimetric SAR data. *IEEE Trans. Geosci. Remote Sens.* **2002**, *40*, 687–698.
18. Hajnsek, I.; Pottier, E.; Cloude, S.R. Inversion of surface parameters from polarimetric SAR. *IEEE Trans. Geosci. Remote Sens.* **2003**, *41*, 727–744.
19. Thiel, C. Extrahierung Hydrologisch Relevanter Parameter aus Hochaufgelösten Polarimetrischen L-BandSowie Interferometrischen X-Band SAR-Daten. Ph.D. Thesis, Friedrich-Schiller-Universität Jena, Jena, Germany, 14 July 2004.
20. Boerner, W.M.; Foo, B.Y.; Eom, H.J. Interpretation of the polarimetric co-polarization phase term in radar images obtained with the JPL airborne L-band SAR system. *IEEE Trans. Geosci. Remote Sens.* **1987**, *25*, 77–82.
21. Ulaby, F.T.; Held, D.; Dobson, M.C.; McDonald, K.C.; Senior, T.B.A. Relating polarization phase difference of SAR signals to scene properties. *IEEE Trans. Geosci. Remote Sens.* **1987**, *25*, 83–92.
22. Wang, J.R.; Mo, T. The polarization phase differences in orchard trees. *Int. J. Remote Sens.* **1990**, *11*, 1255–1265.
23. McNeill, S.; Pairman, D. Stand age retrieval in production forest stands in New Zealand using cand L-band polarimetric radar. *IEEE Trans. Geosci. Remote Sens.* **2005**, *43*, 2503–2515.
24. Garestier, F.; Dubois-Fernandez, P.C.; Guyon, D.; Le Toan, T. Forest biophysical parameter estimating using L-band and P-band polarimetric SAR data. *IEEE Trans. Geosci. Remote Sens.* **2009**, *47*, 3379–3388.
25. Baker, J.R.; Luckman, A.J. Microwave observations of boreal forests in the NOPEX area of Sweden and a comparison with observations of a temperate plantation in the United Kingdom. *Agric. For. Meteorol.* **1999**, *98–99*, 389–416.
26. Watanabe, M.; Shimada, M.; Rosenqvist, A.; Tadono, T.; Matsuoka, M.; Romshoo, S.A.; Furuta, R.; Nakamura, K.; Moriyama, T. Forest structure dependency of the relation between L-band σ^0 and biophysical parameters. *IEEE Trans. Geosci. Remote Sens.* **2006**, *44*, 3154–3165.
27. Goncalves, F.; Santos, J.; Treuhaft, R. Stem volume of tropical forests from polarimetric radar. *Int. J. Remote Sens.* **2011**, *32*, 503–522.
28. Kobayashi, S.; Omura, Y.; Sanga-Ngoie, K.; Widyorini R.; Kawai, S.; Supriadi, B.; Yamaguchi, Y. Characteristics of decomposition powers of L-band multi-polarimetric SAR in assessing tree growth of industrial plantation forests in the tropics. *Remote Sens.* **2012**, *4*, 3058–3077.

29. Yamaguchi, Y.; Moriyama, T.; Ishido, M.; Yamada, H. Four-component scattering model for polarimetric SAR image decomposition. *IEEE Trans. Geosci. Remote Sens.* **2005**, *43*, 1699–1706.
30. Ranson, K.J.; Sun, G. An evaluation of AIRSAR and SIR-C/X-SAR images for mapping northern forest attributes in Maine, USA. *Remote Sens. Environ.* **1997**, *59*, 203–222.
31. Intergovernmental Panel on Climate Change. Volume 4: Agriculture, Forestry and Other Land Use. In *IPCC Guidelines for National Greenhouse Gas Inventories*; Institute for Global Environmental Strategies: Hayama, Japan, 2006.
32. Wagner, W.; Luckman, A.; Vietmeier, J.; Tansey, K.; Balzter, H.; Schmullius, C.; Davidson, M.; Gaveau, D.; Gluck, M.; Le Toan, T.; *et al*. Large-scale mapping of boreal forest in SIBERIA using ERS tandem coherence and JERS backscatter data. *Remote Sens. Environ.* **2003**, *85*, 125–144.
33. Schmullius, C.; Baker, J.; Balzter, H.; Davidson, M.; Eriksson, L.; Gaveau, D.; Gluck, M.; Holz, A.; Letoan, T.; Luckman, A.; *et al*. *SIBERIA—SAR Imaging for Boreal Ecology and Radar Interferometry Applications*; Final Report; Contract No. ENV4-CT97-0743-SIBERIA; Centre for Earth Observations: Jena, Germany, 2001.
34. Balzter, H.; Talmon, E.; Wagner, W.; Gaveau, D.; Plummer, S.; Yu, J.J.; Quegan, S.; Davidson, M.; Le Toan, T.; Gluck, M.; *et al*. Accuracy assessment of a large-scale forest cover map of central Siberia from synthetic aperture radar. *Can. J. Remote Sens.* **2002**, *28*, 719–737.
35. Eriksson, L.; Santoro, M.; Wiesmann, A. Multitemporal JERS repeat-pass coherence for growing stock volume estimation of Siberian forest. *IEEE Trans. Geosci. Remote Sens.* **2003**, *41*, 1561–1570.
36. Thiel, C.J.; Thiel, C.; Reiche, J.; Leiterer, R.; Santoro, M.; Schmullius, C. Polarimetric PALSAR SAR Data for Forest Cover Mapping in Siberia. In Proceedings of First Joint PI Symposium of ALOS Data Nodes for ALOS Science Program, Kyoto, Japan, 19–23 November 2007.
37. Thiel, C.J.; Thiel, C.; Schmullius, C. Operational large-area forest monitoring in Siberia using ALOS PALSAR summer intensities and winter coherence. *IEEE Trans. Geosci. Remote Sens.* **2009**, *47*, 3993–4000.
38. Israelsson, H.; Ulander, L.M.H.; Askne, J.L.H.; Fransson, J.E.S.; Frödlind, P.-O.; Gustavsson, A.; Hellsten, H. Retrieval of forest stem volume using VHF SAR. *IEEE Trans. Geosci. Remote Sens.* **1997**, *35*, 36–40.
39. Cloude, S.R.; Papathanassiou, K.P. Three-stage inversion process for polarimetric SAR interferometry. *Proc. Inst. Elect. Eng. Radar Sonar Navig.* **2003**, *150*, 125–134.
40. Praks, J.; Kugler, F.; Papathanassiou, K.P.; Hajnsek, I.; Hallikainen, M. Height estimation of boreal forest: Interferometric model-based inversion at L- and X-band versus HUTSCAT profiling scatterometer. *IEEE Trans. Geosci. Remote Sens. Lett.* **2007**, *4*, 466–470.
41. Neumann, M.; Saatchi, S.S.; Ulander, L.M.H.; Fransson, J.E.S. Assessing performance of L- and P-band polarimetric interferometric SAR data in estimating boreal forest above-ground biomass. *IEEE Trans. Geosci. Remote Sens.* **2012**, *50*, 714–726.
42. Federal Forest Service of Russia (FFSR). *Manual of Forest Inventory and Planning in Forest Fund of Russia, Part 1*; FFSR: Moscow, Russia, 1995.
43. Weather Underground. Available online: www.wunderground.com (accessed on 7–8 June 2010).
44. Shimada, M.; Isoguchi, O.; Tadono, T.; Isono, K. PALSAR radiometric and geometric Calibration. *IEEE Trans. Geosci. Remote Sens.* **2009**, *47*, 3915–3932.

45. Lee, J.S.; Grunes, M.R.; de Grandi, G. Polarimetric SAR speckle filtering and its implication for classification. *IEEE Trans. Geosci. Remote Sens.* **1999**, *37*, 2363–2373.
46. Freeman, A. Calibration of linearly polarized polarimetric SAR data subject to Faraday rotation. *IEEE Trans. Geosci. Remote Sens.* **2004**, *42*, 1617–1624.
47. Lee, J.S.; Ainsworth, T.L. The effect of orientation angle compensation on coherency matrix and polarimetric target decomposition. *IEEE Trans. Geosci. Remote Sens.* **2011**, *49*, 53–64.
48. Fransson, J.E.S.; Smith, G.; Askne, J.; Olsson, H. Stem volume estimation in boreal forest using ERS-1/2 coherence and SPOT XS optical data. *Int. J. Remote Sens.* **2001**, *22*, 2777–2791.
49. Santoro, M.; Askne, J.; Smith, G.; Fransson, J. Stem volume retrieval in boreal forests from ERS-1/2 interferometry. *Remote Sens. Environ.* **2002**, *81*, 19–35.
50. Rauste, Y. Multi-temporal JERS SAR data in boreal forest biomass mapping. *Remote Sens. Environ.* **2005**, *97*, 263–275.
51. Santoro, M.; Cartus, O. *STSE BIOMASAR: Validating a Novel Biomass Retrieval Algorithm Based on Hyper-Temporal Wide-Swath and Global Monitoring ENVISAT ASAR Datasets*; Final Report; ESA ESRIN Contract No. 21892/08/I-EC; ESA-ESRIN, Centre For Earth Observation: Rome, Italy, 2010.
52. Yamaguchi, Y.; Sato, A.; Boerner, W.M.; Yamada, H. Four-component scattering power decomposition with rotation of coherency matrix. *IEEE Trans. Geosci. Remote Sens.* **2011**, *49*, 2251–2258.
53. Luckman, A.J.; Baker, J.R; Honzák, M.H.; Lucas, R.M. Tropical forest biomass density estimation using JERS-1 SAR: Seasonal variation, confidence limits and application to image mosaics. *Remote Sens. Environ.* **1998**, *63*, 126–139.
54. Fransson, J.E.S.; Israelsson, H. Estimation of stem volume in boreal forests using ERS-1 C- and JERS-1 L-band SAR data. *Int. J. Remote Sens.* **1999**, *20*, 123–137.
55. Askne, J.; Santoro, M.; Smith, G.; Fransson, J.E.S. Multitemporal repeat-pass SAR interferometry of boreal forests. *IEEE Trans. Geosci. Remote Sens.* **2003**, *41*, 1540–1550
56. Luckman, A.J.; Baker, J. R.; Wegmüller, U. Repeat-pass interferometric coherence measurements of disturbed tropical forest from JERS and ERS satellites. *Remote Sens. Environ.* **2000**, *73*, 350–360.
57. Li, Y.; Cao, F.; Hong, W. Limitations in the Polarization Orientation Shift Estimation Using L Band POLSAR Data. In Proceedings of 2009 IET International Radar Conference, Gulin, China, 20–22 April 2009.
58. Saatchi, S.S.; McDonald, K.C. Coherent effects in microwave backscattering models for forest canopies. *IEEE Trans. Geosci. Remote Sens.* **1997**, *35*, 1032–1044.
59. Sun, G.; Simonett, D.S.; Strahler, A.H. A radar backscatter model for discontinuous coniferous forests. *IEEE Trans. Geosci. Remote Sens.* **1991**, *29*, 639–650.
60. Pulliainen, J.T.; Kurvonen, L.; Hallikainen, M.T. Multitemporal behavior of L-band and C-band SAR observations of boreal forests. *IEEE Trans. Geosci. Remote Sens.* **1999**, *37*, 927–937.
61. Ranson, K.J.; Sun, G. Mapping biomass of a northern forest using multifrequency SAR data. *IEEE Trans. Geosci. Remote Sens.* **1994**, *32*, 388–396.

62. Way, J.; Rignot, E.J.M.; McDonald, K.C.; Oren, R.; Kwok, R.; Bonan, G.; Dobson, M.C.; Viereck, L.A.; Roth, J.E. Evaluating the type and state of Alaska taiga forests with imaging radar for use in ecosystem models. *IEEE Trans. Geosci. Remote Sens*. **1994**, *32*, 353–370.
63. Kwok, R.; Rignot, E.J.M.; Way, J.; Freeman, A.; Holt, J. Polarization signatures of frozen and thawed forests of varying environmental state. *IEEE Trans. Geosci. Remote Sens*. **1994**, *32*, 371–381.
64. Dobson, M.G.; McDonald, K.; Ulaby, F.T. Effects of Temperature on Radar Backscatter from Boreal Forests. In Proceedings of IEEE International Symposium Geoscience and Remote Sensing (IGARSS'90), College Park, MD, USA, 20–24 May 1990; pp. 2481–2484.